

1 Lithological control on the landscape form of the Upper  
2 Rhône basin, Central Swiss Alps

3

4 **Laura Stutenbecker<sup>1</sup>, Anna Costa<sup>2</sup>, Fritz Schlunegger<sup>1</sup>**

5 <sup>1</sup> Institut für Geologie, Universität Bern, Baltzerstrasse 1+3, 3012 Bern, Switzerland

6 <sup>2</sup> Institut für Umweltingenieurwissenschaften, ETH Zürich, Stefano-Frascini-Platz 3, 8093  
7 Zürich, Switzerland

8 Correspondence to: L. Stutenbecker (laura.stutenbecker@geo.unibe.ch)

## 9 **Abstract**

10 The development of topography depends mainly on the interplay between uplift and erosion.  
11 These processes are controlled by various factors including climate, glaciers, lithology,  
12 seismic activity and short-term variables, such as anthropogenic impact. Many studies in  
13 orogens all over the world have shown how these controlling variables might affect the  
14 landscape's topography. In particular, it has been hypothesized that lithology exerts a  
15 dominant control on erosion rates and landscape morphology. However, clear demonstrations  
16 of this influence are rare and difficult to disentangle from the overprint of other signals such  
17 as climate or tectonics.

18 In this study we focus on the upper Rhône basin situated in the Central Swiss Alps in order to  
19 explore the relation between topography, possible controlling variables, and lithology in  
20 particular. The Rhône basin has been affected by spatially variable uplift, high orographically  
21 driven rainfalls, and multiple glaciations. Furthermore, lithology and erodibility vary  
22 substantially within the basin. Thanks to high-resolution geological, climatic and topographic  
23 data the Rhône basin is a suitable laboratory to explore these complexities.

24 Elevation, relief, slope and hypsometric data as well as river profile information from digital  
25 elevation models are used to characterize the landscape's topography of around 50 tributary  
26 basins. Additionally, uplift over different time scales, glacial inheritance, precipitation  
27 patterns and erodibility of the underlying bedrock are quantified for each basin.

28 Results show that the chosen topographic and controlling variables vary remarkably between  
29 different tributary basins. We investigate the link between observed topographic differences  
30 and the possible controlling variables through statistical analyses. Variations of elevation,  
31 slope and relief seem to be linked to differences in long-term uplift rate, whereas elevation  
32 distributions (hypsometry) and river profile shapes might be related to glacial imprint. This  
33 confirms that the landscape of the Rhône basin has been highly pre-conditioned by (past)  
34 uplift and glaciation. Linear discriminant analyses (LDA), however, suggest a stronger link  
35 between observed topographic variations and differences in erodibility. We therefore  
36 conclude that despite evident glacial and tectonic conditioning, a lithologic control is still  
37 preserved and measurable in the landscape of the Rhône tributary basins.

## 38 **1. Introduction**

### 39 **1.1 Motivation of this study**

40 The world's topographies have been formed by rock uplift, which is initiated by lithospheric  
41 processes such as plate convergence, collision and crustal thickening (England & Molnar,  
42 1990). However, topographic growth on Earth is not indefinite, but limited by erosional  
43 feedback mechanisms. Once threshold topography has been reached, any further rock uplift  
44 (material input) will be balanced by denudation (material output), and this concept is known  
45 as topographic steady-state (e.g., Adams, 1980; Stüwe et al., 1994; Willett & Brandon, 2002,  
46 and many more). In order to understand this interplay, it is crucial to explore the mechanisms  
47 controlling erosion in an area. In this context, several studies have illustrated that denudation  
48 and landscape form are highly variable in space and time, and that the related topographies  
49 depend on a large number of variables, such as climate, glaciation, tectonics, and lithology.  
50 For example, climate and denudation are coupled in such way that increased precipitation  
51 yields higher river discharges, which in turn tend to enhance rates of fluvial channel incision  
52 (e.g. Willett, 1999; Willett et al., 2006). Rainfall intensity, paired with the total amount of  
53 precipitation, plays an important role in erosional processes by driving hillslope erosion (e.g.  
54 Wischmeier, 1959) and by contributing to the triggering of mass wasting events that are  
55 responsible for mobilizing large amounts of sediment (e.g. Bennett et al., 2012). Glacial  
56 carving was found to be even more efficient than fluvial erosion, particularly where glaciers  
57 have relatively high sliding rates and high basal shear stresses, and where subglacial water  
58 pressure gradients are large (e.g. Hallett et al., 1996; Montgomery, 2002; Norton et al.,  
59 2010a;b; Spotila et al., 2004; Shuster et al., 2005; Valla et al., 2011; Jansen et al., 2014). This  
60 seems to be especially valid for the Quaternary period, when multiple glacial advances and  
61 retreats have formed the mountainous landscapes in many orogens (e.g. Kelly et al., 2004).  
62 On an orogen-wide scale, other authors have reported that the tectonic control on denudation  
63 and landscape form has been more pronounced than climate. For example, periods of  
64 accelerated uplift in the Alps around 5 million years ago, recorded by apatite fission track  
65 ages (Michalski & Soom, 1990; Vernon et al., 2008, Fox et al., 2015), coincide with a  
66 generally higher sediment flux into the foreland basin (Kuhlemann et al., 2002). Besides a  
67 possible climatic driver, deep-crustal processes such as unbending and unloading of the  
68 subducting slab have been taken into account to explain this large-scale phenomenon (Sue et  
69 al. 2007; Baran et al. 2014; Fox et al., 2015). Wittmann et al. (2007) measured Holocene  
70 erosion rates in Alpine river sediments, which correlate very well with geodetic-based rock

71 uplift rates. These relationships have been used to suggest that vertical movement of rock has  
72 mainly been caused by isostatic compensation of removed material (Champagnac et al.,  
73 2009). In thematically related studies, several authors concluded that erosion rates directly  
74 correlate with geomorphological variables like slope gradients and local as well as basin-  
75 scale relief that can be extracted from digital elevation models (Granger et al., 1996; Schaller  
76 et al., 2001; Montgomery & Brandon, 2002). Finally, lithology and related rock-mass  
77 strengths have been considered as additional factors controlling denudation and particularly  
78 landscape forms, since soft lithologies like marls are eroded faster than hard lithologies such  
79 as granites or gneisses, and mechanically stronger rocks can sustain steeper slopes (e.g.  
80 Molnar et al., 2007; Korup and Schlunegger, 2009; Korup & Weidinger, 2011; Korup, 2008;  
81 Morel et al., 2003; Cruz Nunes et al., 2015; Scharf et al., 2013).

82 The Central European Alps have been intensively studied on how surface and crustal-scale  
83 processes have been coupled through time, and how effects related to these mechanisms have  
84 been modulated by glacial erosion and deposition (e.g. Persaud & Pfiffner, 2004;  
85 Gudmundsson, 1994; Champagnac et al., 2007; Schlunegger & Hinderer, 2001; Cederbom et  
86 al., 2011; Norton et al., 2010b; Schlunegger & Norton, 2013). However, much less attention  
87 has been paid to exploring how the tectonic architecture, and the nature of the bedrock  
88 lithology in particular, has driven surface erosion and has conditioned the shape of the Alpine  
89 landscape (Kühni & Pfiffner, 2001; Norton et al., 2010b), mainly because the spatial and  
90 temporal variability of uplift, climate, glacial cover and lithology (Schmid et al., 1996; Kühni  
91 & Pfiffner, 2001; Bini et al., 2009) complicates an integrated understanding of the erosional  
92 patterns and the resulting landscape form in this orogen. Nevertheless, because of the obvious  
93 spatial variation in bedrock lithology, the Alps offer an ideal laboratory to explore whether  
94 landscape properties at the basin scale (mean elevation, hypsometry, relief, hillslope gradients  
95 and stream profile shapes) are mainly grouped around identical lithologies, or other  
96 conditions and driving forces (long- and short-term uplift, climate, etc.). It is the scope of this  
97 paper to explore these possibilities.

98 Here, we focus on the upper Rhône basin in south-western Switzerland, which is the largest  
99 inner-alpine drainage system with a total catchment size of around 5500 km<sup>2</sup>. The Rhône  
100 basin was covered by some of the thickest Alpine glaciers during multiple glaciations  
101 throughout the Quaternary (Kelly et al., 2004; Bini et al., 2009) and has recently experienced  
102 some of the highest uplift rates in the Alps (Kahle et al., 1997; Schlatter et al., 2005). In  
103 particular, we test whether the major spatially variable attributes that have been used to

104 characterize a topography at the basin scale including: mean elevation, relief, slope,  
105 hypsometry, and longitudinal profiles of streams bear information that can be related to any  
106 of the variables conditioning or controlling erosion including: uplift across timescales,  
107 climate, LGM glaciation and lithology. To this extent, we compile topographic data from  
108 around 50 tributary basins feeding the Rhône River between its source, the Rhône glacier,  
109 and its terminus, defined here by the delta at Lake Geneva (figure 1). We complement our  
110 topographic data with published large-scale geological, climatic, glacial (LGM thickness) and  
111 exhumation data in order to attain a large-scale understanding of the predominant processes  
112 controlling the landscape's form of this basin over multiple scales. We find distinct spatial  
113 differences in the landscape's properties, which can be related to the erodibility of the  
114 bedrock. This suggests that underlying lithology has exerted a fundamental control on erosion  
115 and the resulting landscape form.

## 116 **1.2 Organization of the paper**

117 We base our analyses on previous studies where uplift (long- and short-term), glacial  
118 inheritance, precipitation and erosional resistance of the underlying bedrock have been  
119 invoked to explain the landscape's characteristics, expressed through variables such as: mean  
120 elevation, hypsometry, relief, hillslope gradients and longstream profiles (Kühni and Pfiffner,  
121 2001; Wittmann et al., 2007; Norton et al., 2010; Schlunegger and Norton, 2013). We test  
122 these relationships through correlation and statistical analyses, and we conclude that  
123 variations in erodibility explain most of the morphometric variations that we can observe  
124 within the Rhône basin.

## 125 **2. Geological setting**

### 126 **2.1 Geology**

127 The study area covers the entire upper Rhône catchment between the Rhône glacier and Lake  
128 Geneva in the central Swiss Alps (figure 1).

129 *Figure 1: Location map of the study area showing the main Rhône River and 55 main*  
130 *tributary streams ( $>10\text{km}^2$ ) that are analysed in this study.*

131

132 The bedrock of the upper Rhône basin comprises the major tectonic units of the western  
133 Alpine orogen (e.g. Froitzheim et al., 1996; Schmid et al., 2004). Along its ca. 160 km long  
134 course from its source next to the Grimselpass at over 2000 m a.s.l. towards the delta on Lake  
135 Geneva at c. 370 m a.s.l., c. 50 major tributary streams with sources in either Penninic units,

136 Helvetic nappes or crystalline basement rocks derived from the European continental and  
137 oceanic lithosphere (Schmid et al., 2004) discharge their material into the Rhône River. The  
138 related lithologies are oceanic metasedimentary and ophiolitic rocks exposed in the Penninic  
139 nappes covering 52% of the total Rhône watershed. These units are mostly drained by  
140 tributaries south of the main Rhône valley (figure 2a). Variscan crystalline rocks of the  
141 European basement (granites, gneisses and schists) of the Aar, Aiguilles-Rouges and Mont-  
142 Blanc External massifs, exposed on both the eastern and western sides of the Rhône valley,  
143 contribute to 22% of the bedrock underlying the Rhône basin. Calcareous metasedimentary  
144 rocks of the European continental margin are exposed in the Helvetic and Ultrahelvetic  
145 nappes north of the main Rhône valley and make up c. 16% of the total watershed. Finally,  
146 minor proportions of the Rhône watershed are made of unconsolidated Quaternary (6%) and  
147 Oligocene Molasse (1%) units as well as the “Sub-Penninic” basement nappes of the  
148 Gotthard massif (3%).

149 Kühni & Pfiffner (2001) reconstructed a large-scale erodibility map for the Swiss Alps,  
150 which is mainly based on the geological and geotechnical map of Switzerland (Niggli & de  
151 Quervain, 1936). These authors used detailed field observations, frequency of landslides, as  
152 well as structural and topographic parameters from the Rhine basin (Jäckli, 1957) situated in  
153 the eastern Swiss Alps for calibration purposes, based on which erodibility classes were  
154 assigned to distinct lithologies (figure 2b). Lithologies with a very high erodibility are mainly  
155 encountered in Molasse and Flysch deposits. A medium erodibility has been assigned to  
156 Mesozoic carbonates that are exposed in e.g., the Helvetic nappes and Penninic Klippen belt.  
157 Paragneisses are considered to have a low erodibility, while the lowest erodibility has been  
158 assigned to orthogneisses, amphibolites and granitoid rocks that are currently exposed e.g. in  
159 the Aar massif.

160

161 *Figure 2:*

162 *a) Simplified litho-tectonic map of the study area showing the major paleogeographic*  
163 *domains, the Helvetic nappes (blue), the Penninic nappes (green) and the External massifs*  
164 *(red) and the major structural features (data compilation from swisstopo© geological map*  
165 *1:500000)*

166 *b) Erodibility map after Kühni & Pfiffner (2001), based on Niggli & de Quervain (1936) and*  
167 *Jäckli (1957) showing the general erodibility of bedrock*

168        **2.2 Tectonics**

169    The tectonic setting of the Rhône basin is dominated by the Rhône-Simplon fault system,  
170    where dextral strike-slip movements since early Miocene times have accommodated most of  
171    the orogenic extension (Schlunegger & Willett, 1999; Egli & Mancktelow, 2013). Seward &  
172    Mancktelow (1994) suggested that faulting also had a normal slip component, which played  
173    an important role in the younger exhumation history of the area. The Rhône-Simplon fault is  
174    not only the boundary between two different paleogeographic domains, but also separates  
175    two terrains with significantly different exhumation histories (Michalski & Soom, 1990;  
176    Schlunegger & Willett, 1999; Vernon et al., 2008; and references within, figure 3a). In  
177    particular, south of this fault in the Penninic domain, apatite fission-track ages range between  
178    8 and 20 million years. In contrast, north of the fault in the Aar massif and the overlying  
179    Helvetic nappes, related exhumation ages are considerably younger (1.5-12 million years).  
180    The External massifs such as the Aar and the Mont Blanc massif have been exhumed in  
181    Neogene times up to 8 km in  $\leq 15$  Ma (Pfiffner et al., 1997) and therefore show the youngest  
182    exhumation ages of c. 1.5-5 Ma (Michalski & Soom, 1990).

183    Levelling and geodetic surveys revealed that the Rhône basin has experienced some of the  
184    highest uplift rates throughout the entire Alpine orogen during the past years (Kahle et al.,  
185    1997; Schlatter et al., 2005). These high uplift rates were related to a combination of ongoing  
186    collisional processes (Persaud & Pfiffner, 2004), erosional (Champagnac et al., 2009) and  
187    glacial unloading (Gudmundsson, 1994). Uplift rates are highest in the eastern part of the  
188    study area (1.5 mm/a) and decrease to  $< 0.3$  mm/a towards Lake Geneva (figure 3a).

189        **2.3 Glaciation**

190    During the Quaternary, the landscape of the Rhône valley has been shaped and carved by  
191    multiple glaciations (Ivy-Ochs et al., 2008; Valla et al., 2011). In this context, the entire basin  
192    was covered by an up to 1.5-km-thick ice sheet during the Last Glacial Maximum c. 18-24 ky  
193    ago (Kelly et al., 2004; Bini et al., 2009). At the eastern border of the Rhône valley, two  
194    separate ice domes formed the ice divide of the Rhône and the Rhine headwaters (Florineth &  
195    Schlüchter, 1998). The ice drained into the valleys (including the Rhône valley) down to the  
196    foreland in the north, from where the ice thicknesses decreased radially towards the West.

197    The Rhône valley has hosted some of the thickest Alpine glaciers including the Rhône or the  
198    Aletsch glacier. Today, c. 9% of the entire upper Rhône watershed is still glaciated, and most

199 of the glaciers are situated in the East and Southeast of the basin (figure 3b). Their  
200 distribution within the three main litho-tectonic units is very distinct with glacial covers  
201 ranging from a maximum of 17.7% in the Aar massifs, 12.5% in the Penninic units and only  
202 1.5% in the Helvetic nappes. Individual tributary basins like the Massa basin (figure 1) are  
203 glaciated up to 50%, whereas others are completely ice-free. Numerous morphological  
204 features like oversteepened head scarps, wide, U-shaped, deeply carved trunk valleys and  
205 hanging tributary rivers including oversteepened inner gorges reflect the landscape's strong  
206 glacial inheritance (Norton et al., 2010a;b; Valla et al., 2011).

## 207 **2.4 Climate**

208 The spatial distribution of precipitation of the current climate is shown in the form of total  
209 annual precipitation and high intensity rainfall represented by annual 90<sup>th</sup> percentiles of total  
210 daily precipitation. Computations are based on the RhiresD product of the Swiss Federal  
211 Office of Meteorology and Climatology MeteoSwiss (Schwarb, 2000). Within the upper  
212 Rhône basin, annual precipitation is characterized by a rather high variability in space,  
213 ranging from less than 500 mm per year along the Rhône Valley to more than 2500 mm per  
214 year at very high elevations (figure 3c). This spatial pattern is mostly driven by orography  
215 where inner, low elevation, sheltered valleys show relatively dry conditions, while the annual  
216 amount of precipitation is much larger at higher altitudes (e.g., Frei and Schär, 1998).

217 *Figure 3:*

218 *a) Interpolated exhumation ages based on apatite fission-track dating (Vernon et al., 2008)*  
219 *show youngest ages both in the East and the West and a decrease towards the basin outlet at*  
220 *Lake Geneva. Contour lines indicating recent uplift (for the time span 1903-2003) are*  
221 *interpolated from Schlatter et al. (2005) and Kahle et al. (1997).*

222 *b) Map showing the ice thickness during the Last Glacial Maximum (from Bini et al., 2009)*  
223 *and the recent distribution of moraine deposits (glacial till) and glaciers.*

224 *c) Spatial distribution of total annual precipitation averaged over the period 1961-2012*  
225 *based on Schwarb (2000).*

## 226 **3. Methodology and Database**

227 Tectonic, climatic and glacial forcing and their interplay operating at different scales through  
228 space and time can be identified by the perturbation they have caused in the landscape. The



229 landscape's response and related morphologic measures can then be suggestive for extents at  
230 which re-equilibrations to those perturbations have proceeded (e.g., Robl et al., 2015, for the  
231 case of the European Alps). In this context, we extract morphometric data such as elevation,  
232 relief, slope, hypsometry and river long profiles from a digital elevation model (DEM)  
233 distributions to characterize the landscape at the basin scale (e.g., Wobus et al., 2006;  
234 Brocklehurst & Whipple, 2004; Champagnac et al. 2012; Robl et al., 2015). We then test the  
235 possible relation of these topographic variables to external forcing mechanisms such as uplift,  
236 precipitation, glacial inheritance and erodibility through distribution and linear discriminant  
237 analyses.

### 238 **3.1 Topographic variables**

239 All topographic variables including measures for elevation, slope gradients and river profile  
240 shapes (at the tributary basin scale) were extracted with standard geomorphological and  
241 hydrological tools in ArcGIS© version 10.1. The base dataset for all analyses was the 2-m-  
242 resolution digital elevation model (DEM) swissALTI<sup>3D</sup> generated by the Swiss Federal  
243 Office of Topography (swisstopo) in 2014.

#### 244 3.1.1 Mean elevation, Relief and Slopes

245 We calculated mean elevation within each basin from the 2m-resolution DEM.  
246 The local relief corresponds to the difference between the highest and the lowest point of  
247 elevation in a defined area (Ahnert, 1984). Because the studied tributary basins have  
248 significantly different catchment sizes (ca. 10-700 km<sup>2</sup>), it is not meaningful to calculate the  
249 local relief over the entire catchment. For a better comparability, we instead chose a 1-km-  
250 diameter circular sampling window, in which the mean elevation difference is calculated  
251 using focal statistics (Montgomery & Brandon, 2002; Korup et al., 2005). Finally, slope  
252 values were calculated in ArcGIS© with the imbedded slope algorithm from the 2-m-DEM.  
253 We excluded currently glaciated areas from the calculation, because they would bias the  
254 results towards higher frequencies of lower slopes. Mean slope values were then calculated  
255 from this database for each tributary basin.

#### 256 3.1.2 Hypsometry

257 We used the hypsometric integral (Strahler, 1952) as measure for the distribution of  
258 elevations within the catchments. In particular, the hypsometry of a basin can be used to infer  
259 the stage at which the landscape has evolved, where progressive erosion will continuously  
260 lower the overall topography and elevations will be skewed towards lower values (Strahler,

261 1952; Brozović et al., 1997). The hypsometric integral (HI) can be expressed as the integral  
262 below the hypsometric curve, which in turn represents the proportion of a basin that lies  
263 below a given elevation (Hurtrez et al., 1999). The hypsometric curve displays normalized  
264 elevations on the ordinate and normalized cumulative area above the corresponding elevation  
265 on the abscissa. The convexity of the shape of this curve increases (and corresponding HI  
266 values are accordingly higher) as the distribution of elevations are skewed towards higher  
267 values. In contrast, s-shaped or concave hypsometric curves and lower HI values occur in  
268 more evolved landscapes, where erosional processes have preferably removed areas of high  
269 elevation (Brozović et al., 1997; Brocklehurst & Whipple, 2002; 2004; Montgomery et al.,  
270 2001). Accordingly, we calculated the HI for each watershed  $>10 \text{ km}^2$  using a bin size of 100  
271 m suitable for hypsometric analyses through eq. (1):

272

$$273 \quad HI = \frac{H_{mean} - H_{min}}{H_{max} - H_{min}} \quad (\text{Eq. 1}),$$

274 where  $H_{mean}$ ,  $H_{min}$  and  $H_{max}$  refer to the mean, minimum and maximum elevation of the basin.

### 275 3.1.3 River profiles

276 Several authors have quantified the concavity of longitudinal river profiles (e.g., Whipple &  
277 Tucker, 1999; Whipple, 2004; Wobus et al., 2006) through the application of Flint's law  
278 (Flint, 1974), where the local channel gradient  $S$  is related to the upstream drainage area  $A$   
279 through (eq. 2):

$$280 \quad S = k_s \cdot A^{-\theta} \quad (\text{Eq. 2})$$

281 Here, the coefficient  $k_s$  corresponds to the steepness index, while the exponent  $\theta$  is referred to  
282 as the concavity index. In case of normally graded stream profiles,  $S$  and  $A$  show a linear  
283 relationship in log/log plots (figure 4). The slope of this linear regression line corresponds to  
284 the concavity index  $\theta$ , while the intercept with the y-axis is the value of the steepness index  
285  $k_s$ .

286 Longitudinal river profiles were extracted from the hydrologically filled 2-m-DEM provided  
287 by Swisstopo using ArcGIS© 10.1 and the Matlab© based TopoToolbox by Schwanghart &  
288 Kuhn (2010). The code calculates the hydrologic flow into each pixel, and based on this  
289 extracts the main channel of the river (i.e., the pixels in which the hydrologic flow is largest).  
290 Along the main channel, elevation and distance, as well as slope and upstream area are

291 extracted in order to plot the river profile and the slope/area relation, respectively.  $\Theta$  and  $k_s$   
292 are then calculated through linear regressions of the slope/area plot. We performed this  
293 regression over the entire stream length to allow better comparison between the different  
294 streams (e.g., Korup, 2008).

295 *Figure 4: Exemplary plot showing the linear regression of the logarithmic slope/area plot, of*  
296 *which the two variables  $\theta$  and  $k_s$  can be derived.*

297

## 298 **3.2 Possible controlling and conditioning variables**

299 Parameters are referred to as controlling or conditioning variables if they have been used to  
300 explain the topographic development of the Rhône drainage basin across scales including:  
301 uplift (Wittmann et al., 2007), precipitation and/or glacial inheritance (Schlunegger and  
302 Norton, 2013) and erodibility (Kühni and Pfiffner, 2001). These variables potentially explain  
303 the patterns of first-order morphometric variables outlined above. We assign quantitative  
304 values for the four variables to each tributary basin, using published maps as basis (see  
305 chapter 2).

### 306 3.2.1 Uplift

307 We consider two different time scales by exploring the controls of rock uplift on the  
308 landscape of the Rhône. First, patterns of long-term exhumation and related rock uplift can be  
309 extracted from apatite fission track cooling ages (section 1.2). Accordingly, for each tributary  
310 basin, we calculate mean cooling-ages based on the map by Vernon et al. (2008). The  
311 tributary basins are then categorized using a ternary division into relatively recent (1.5-5 My),  
312 intermediate (5-8 My) and old (>8 My ago) cooling ages. This division approximately  
313 follows the assignment to classes by Vernon et al. (2008).

314 To account for recent surface uplift rates, we use the data provided by Schlatter et al. (2005),  
315 which we interpolated along the study area. This dataset is based on geodetic levelling  
316 surveys conducted for around 10'000 control points over Switzerland by the Swiss Federal  
317 Office of Topography between ~1903 and 2003. We divide recent surface uplift into three  
318 intervals including low (0.5-0.9 mm/a), intermediate (0.9-1.4 mm/a) and high (1.4-1.6 mm/a)  
319 rates and assign related classes to each tributary basin.

### 320 3.2.2 Precipitation

321 The distribution of respectively total annual precipitation (amount) and annual 90<sup>th</sup>  
322 percentiles (intensity) of total daily precipitation are used to characterize modern  
323 precipitation rates and patterns respectively. Computations are based on the RhiresD product  
324 of the Swiss Federal Office of Meteorology and Climatology MeteoSwiss (Schwarb, 2000).  
325 RhiresD is a gridded daily precipitation dataset covering the Swiss territory with a spatial  
326 resolution of ~2x2 km from 1961 to present. Computations are conducted directly on the  
327 native grid and are consecutively distributed over a 250x250 m grid by proximal  
328 interpolation. The precipitation amount and 90<sup>th</sup> percentile of total daily precipitation were  
329 calculated on annual basis and averaged over the 52 year period 1961-2012 for each  
330 catchment. Quantiles are computed only for wet days, assuming a threshold of 1 mm/day for  
331 distinguishing wet and dry days.

332 For the precipitation amount, we divide the basins into three evenly spaced classes: 975-  
333 1340, 1340-1840 and 1840-2278 mm/y. For the precipitation intensity indicated by the 90<sup>th</sup>  
334 percentile, we also divide the basins into three evenly spaced classes: 19-25, 25-31 and 31-37  
335 mm/day.

336

### 337 3.2.3 Glacial inheritance

338 The glacial extent during the LGM and related patterns of ice thickness (Florineth &  
339 Schlüchter, 1998; Kelly et al., 2004; Bini et al., 2009) is used, mainly because this variable  
340 has been used to explain some of the landscape forms in the Central European Alps  
341 (Schlunegger & Norton, 2013). We calculate LGM-related ice volumes within each tributary  
342 basin by subtracting today's landscape elevation (derived from the DEM) from the LGM  
343 surface map by Bini et al. (2009). Areas that were above the ice during the LGM are  
344 excluded from the resulting map. We calculate mean values of the resulting ice thickness for  
345 each tributary basin and classify them into three evenly spaced intervals, 167-292, 292-471  
346 and 471-651 m.

### 347 3.2.4 Erodibility

348 We use the erodibility classes defined by Kühni & Pfiffner (2001) (see section 2.1) as a  
349 measure for the erosional resistance of the underlying bedrock. Flysch and Molasse deposits  
350 are assigned a high erodibility (1). Mesozoic carbonates as they occur in the Helvetic nappes  
351 have a medium erodibility (2). Paragneisses and other poly-metamorphic rocks that are  
352 exposed mainly in the Penninic nappes and subordinately in the External massifs have a low

353 erodibility (3). Very low erodibility values (4) have been assigned to granitoid rocks and  
354 orthogneisses. These rock types are common in the External massifs and subordinate in the  
355 Penninic nappes. Since most of the basins comprise rocks of different erodibilities (figure  
356 2b), we calculate mean values for each basin thereby considering the relative proportion of  
357 erodibility classes per basin, and group them in high (1-2), low (2-3) and very low (3-4).  
358 This division would need to be more precise on a smaller scale to allow the consideration of  
359 small-scale lithological variation. However, for our basin-wide approach, we found this  
360 division sufficiently precise.

### 361 **3.3 Correlation, distribution and statistical analysis**

362 Possible relationships between the topographic and the controlling variables are explored  
363 through regression analyses, where correlation strengths for each pair of variables are  
364 expressed by the square of the correlation coefficient,  $r^2$ .  $r^2$  values  $>0.5$  are considered to  
365 indicate a strong correlation, while values between 0.3-0.5 indicate weak correlation. No  
366 causal relationships are assigned for pairs with correlation  $<0.3$ . Several authors found that in  
367 some of the topographic measures analysed here may depend on basin size rather than on  
368 external forcing mechanisms (e.g., Willgoose & Hancock, 1997; Korup et al., 2005; Cheng et  
369 al., 2012). Since the tributary basins in the study area show quite a large range between ca. 10  
370 -  $>700\text{km}^2$ , we also test possible dependencies of all topographic variables on basin size.

371 We then analyse the relation between the topographic and the controlling variables. To  
372 achieve this, all topographic variables are plotted in sets of boxplots for each controlling  
373 variable. The boxplots display the general range of the data, including the maximum and  
374 minimum values, the median, the upper and lower quartile, and outliers. These statistical  
375 measures help describing the general data distribution and their scatter. Furthermore, they  
376 allow for the comparison of the distribution of data between defined classes, and help to  
377 identify whether there are significant differences.

378 We finally test whether the topographic variables of the studied basins are sufficient to  
379 predict the affiliations of the basins through linear discriminant analyses (LDA). In contrast  
380 to principal component analysis, LDA takes into account the affiliation of a sample to a  
381 certain group (McLachlan, 2004), in our case for example basins with similar uplift rates or  
382 low erodibility. Therefore, LDA allows testing whether a basin has been assigned correctly to  
383 a group (e.g. high uplift rate) based on its topographic characteristics. In addition, because the  
384 LDA reduces the dimensions of the data to a linear space, related results can be displayed in a

385 two-dimensional scatter plot, where each sample is defined by two eigenvectors (McLachlan,  
386 2004). The distinct groups should then be visible as clusters in this plot if the topographic  
387 variables are significantly different between the groups of the chosen category. Furthermore,  
388 the LDA approach yields in prediction of the affiliation of a sample to a group based on the  
389 eigenvalues inferred from the variables, and it allows the comparison of these results with the  
390 actual group affiliation.

391

## 392 **4. Results**

### 393 **4.1 Values and correlations**

394 Most topographic variables show a relatively large scatter between the analysed catchments  
395 (see table 1). Mean elevations range between ca. 1420 and 2890 m a.s.l.. The mean values of  
396 relief calculated for 1 km- radii range between 470-990 m, while slopes are between 19.5°  
397 and 40.7° steep on the average. The hypsometric integral has a mean value of 0.45, but  
398 scatters widely between 0.28 and 0.70 for the individual tributary basins. The river long  
399 profiles also show a wide variety in shape (figure 5). They display almost undisturbed  
400 concave, over s-shaped (concave-convex) with knickpoints to almost completely convex  
401 profiles. Accordingly, the  $\theta$  and  $k_s$  values yield large scatters. Most important, nearly all river  
402 profiles have features indicative for topographic transient states such as multiple knickzones  
403 and convexities (figure 5).

404 Most topographic variables show no or only weak correlation ( $r^2 < 0.3$ , see figure 6) with one  
405 another. Only the pairs of slope/relief and HI/ $\theta$  are characterized by a strong positive  
406 correlation with values of  $r^2 > 0.5$ . No statistically significant correlations between any of the  
407 topographic variables and basin size were observed (all  $r^2 < 0.3$ ).

408 For the controlling variables, table 2 shows the extracted values for each basin based on the  
409 categorization described in chapter 3.2. There exists a strong correlation between the two  
410 measures of precipitation ( $r^2 = 0.710$ , figure 7). Since all other variable pairs have  $r^2$  values  
411 below 0.3, they can be considered as not strongly correlated. Note that also for basin size  
412 there is no statistically significant correlation between any of the analysed variables (figure  
413 7).

414 *Table 1: Topographic variables (section 2.1) extracted for the studied catchments*

415 *Table 2: Possibly controlling variables (2.2) extracted for the studied catchments.*

416 *Figure 5: Longitudinal river profiles with normalized distance and elevation.*

417 *Figure 6: Correlation matrix of the topographic variables extracted from the DEM (mean*  
418 *elevation, relief, slope, HI, concavity, ks) and basin size. The strength of correlation for each*  
419 *pair is given by the coefficient of determination,  $r^2$ .*

420 *Figure 7: Correlation matrix of the possibly controlling variables uplift (short- and long-*  
421 *term), precipitation (annual mean and 90<sup>th</sup> percentile), LGM ice thickness and erodibility.*  
422 *The strength of correlation for each pair is given by the square of the correlation coefficient,*  
423  *$r^2$ .*

#### 424 **4.2 Distribution analysis in boxplots**

425 Each set of boxplots (figures 8-13) displays the topographic variables grouped into the three  
426 sub-classes defined for each of the controlling variables.

427 The mean apatite fission-track ages for each catchment can be used as a proxy for the long-  
428 term uplift history (Vernon et al., 2008). Figure 8 shows that the topographic variables  
429 generally group into these three classes (<5 My, 5 – 8 My, and >8 My; see above and Vernon  
430 et al., 2008), albeit with a large scatter. Catchments characterized by relatively old apatite  
431 ages show generally lower elevation, relief and slope values. Conversely, catchments yielding  
432 young apatite ages show the highest values of elevations, relief and slopes. In contrast,  
433 hypsometric integrals and river profile shapes do not show any variation between the three  
434 sets of fission track ages.

435 Short-term uplift rates, which have been quantified using geodetic data collected over the past  
436 century (Schlatter et al., 2005), yield a similar pattern regarding relationships with  
437 topographic metrics. Elevation, relief and slope values tend to increase with increasing  
438 surface uplift rate (figure 9a,b,c), although the trend is less clear than in case of the long-term  
439 uplift variable. Hypsometric integrals and the river profile shapes show no clear trend with  
440 geodetic uplift rates (figure 9 d,e).

441 Mean ice thickness in each catchment during the LGM can be considered as a measure of  
442 glacial imprint onto the landscape (Schlunegger & Norton, 2013). However, no clear  
443 variations can be observed between the three defined LGM thickness classes and elevation,  
444 relief and slope (figure 10a,b,c). In basins with thicker ice, the HI is clearly lower, and the  
445 river profile concavity higher than in basins with thinner ice (figure 10d,e).

446 Precipitation is quantified by the amount and the intensity of precipitation averaged over the  
447 time span from 1961-2012, for which data record is available. Regarding the amount of  
448 precipitation, topographic variables do not show any clear variation in-between the three  
449 defined precipitation classes (figure 11). The only noticeable relation exists in wet basins  
450 (>1836 mm/y), which are characterized by high elevations. For the intensity of precipitation,  
451 which we express here by the 90<sup>th</sup> percentile of daily precipitation, the results are also non-  
452 distinct (figure 12). However, the basins characterized by very high rainfall intensity show  
453 much steeper slopes than for the basins with less intense precipitation.

454 Topographic variables show a relatively low scatter within the three erodibility groups, which  
455 is expressed by rather small boxes (figure 13). In particular, elevation, relief and slope values  
456 are significantly different between basins with high, medium and low erodibility. The  
457 relationships are less clear for hypsometric integral and river profile shapes.

458 *Figure 8: Boxplots of the topographic variables grouped after the apatite fission-track ages*  
459 *(Vernon et al., 2008), which give long-term uplift information. The boxes represent the areas,*  
460 *in which 50% of the data plot (first and third quartile). The line in the middle is the median of*  
461 *the data. The whiskers mark the maximal and minimal value, and outliers are represented by*  
462 *white dots.*

463 *Figure 9: Boxplots of the topographic variables grouped after the recent uplift rates*  
464 *(Schlatter et al., 2005), which give short-term uplift information.*

465 *Figure 10: Boxplots of the topographic variables grouped after the LGM ice thickness (Bini*  
466 *et al. 2009), which are indicative for glacial inheritance.*

467 *Figure 11: Boxplots of the topographic variables grouped after the amount of precipitation,*  
468 *expressed by the annual mean precipitation.*

469 *Figure 12: Boxplots of the topographic variables grouped after the intensity of precipitation,*  
470 *expressed by the 90<sup>th</sup> percentile of total daily precipitation.*

471 *Figure 13: Boxplots of the topographic variables grouped after erodibility.*

### 472 **4.3 Linear discriminant analysis (LDA)**

473 The LDA classification shows that the best results are generated when erodibility is  
474 considered as a classification basis (table 3). In particular, 80% of all basins are classified



475 correctly on this basis, and the individual correct classification of the three groups ranges  
476 between c. 75% and 85%. In the scatterplots, a clear clustering of the three classes is visible  
477 (figure 14). Basins with low and high erodibilities form distinct point clouds, while basins  
478 with a medium erodibility occur in-between these clouds.

479 In the same sense, geodetic short-term uplift appears to be a good basis for clustering basins  
480 on their landscape metrics, since a total of 76% of basins are correctly classified. However,  
481 basins of group 3 (1.4-1.6 mm/y) are classified correctly only to 44%, which lowers the  
482 overall LDA performance. The clustering is clear in the scatterplots (figure 14). Note,  
483 however, that the cluster of basins of class 3 lays between the ones of class 1 and 2.

484 Regarding the variables long-term uplift, LGM ice thickness and intensity of precipitation  
485 (90<sup>th</sup> percentile), the values of correct classifications range between 62 and 70%. However, in  
486 all three cases, there is always one class that yields a very low percentage of correct  
487 classification. A clustering is hardly visible in the scatterplot for the variable long-term uplift,  
488 and mostly absent for the variables LGM ice thickness and intensity of precipitation. Finally,  
489 with respect to the amount of precipitation, all three classes of this variable yield percentages  
490 around 70% if they are used as categorization basis. However, in the scatterplots, clustering is  
491 rather poor as only class 3 forms a distinguishable point cloud, whereas the other two classes  
492 are indistinct from each other.

493

494 *Figure 14: Scatter plots of the LDA results for long-term uplift (a), recent surface uplift (b),*  
495 *LGM ice thickness (c), amount (d) and intensity (e) of precipitation, and erodibility (f).*

496

497 *Table 3: Results of the LDA classification based on the topographic variables for each of the*  
498 *controlling variables.*

## 499 **5. Discussion**

500 Topographic metrics of tributary basins in the Rhône valley show relationships with all four  
501 controlling mechanisms including uplift, glacial inheritance, precipitation and erodibility. For  
502 example, river basins with a history of relatively fast inferred exhumation rate (apatite FT  
503 cooling age <5 My) have comparably higher elevation, relief and slope values, albeit with  
504 some poor correlations particularly regarding mean elevation and local relief (Fig. 8). This  
505 trend is consistent with studies analysing the relationship between long-term surface uplift  
506 and the development of topography (e.g., Ahnert, 1984; Small & Anderson, 1998;  
507 Brocklehurst & Whipple, 2002). However, we could not find any significant relation between

508 uplift (neither long-term nor short-term), hypsometry and river profile concavity. This  
509 suggests that the distribution of elevations within the basin and the shape of the river profile  
510 have not been influenced by uplift.

511 In contrast, we found a relation between hypsometry, river profile convexity and the LGM ice  
512 thickness, where basins with a thinner ice cover have higher hypsometric integrals and lower  
513  $\theta$  values. Extensively glaciated basins characterized by thicker LGM ice can have lower  
514 equilibrium line altitudes (ELA) than only moderately glaciated basins. This allows a  
515 stronger glacial modification especially in lower regions and thus a lowering of both the  
516 hypsometric curve and integral (Brocklehurst & Whipple, 2004). Ice thickness might  
517 influence the efficiency of glacial erosion in the valley through larger shear stresses driven by  
518 thick ice (Brocklehurst & Whipple, 2002; Dürst Stucki & Schlunegger, 2013). Thicker ice  
519 cover promotes the formation of flat and partially overdeepened lower reaches and steep head  
520 scarps, forming valleys with concave thalwegs. Large glacial erosion driven by thick ice may  
521 also promote fluvial incision during subsequent interglacial times through a positive feedback  
522 response (Norton et al., 2010b), where the landscape's disequilibrium, conditioned by glacial  
523 erosion, promotes fluvial erosion through head ward retreat, thereby increasing the stream's  
524 concavity. This is expected along valley reaches where glacial processes resulted in the  
525 formation of topographic steps. In either case, glacial perturbations paired with fluvial  
526 responses are expected to return thalwegs with larger concavities, which we invoke here to  
527 explain the positive correlations between these variables in the tributary basins of the Rhône  
528 River (Figure 10e). Although variations in LGM ice cover seem to be a valid explanation for  
529 the shape of some of the observed river profiles and the elevation distributions within the  
530 basin (see also Schlunegger and Norton, 2013), we could not detect a relation between ice  
531 thickness and elevation, relief or slope. This suggests that in our study area the degree of  
532 glacial inheritance is not responsible for relief production or ridgeline lowering in the basins,  
533 nor can it be invoked to explain patterns of slope angles, a note that has already been made by  
534 Norton et al. (2010b).

535 Erodibility offers a possible explanation for reconciling some of the lack of correlations  
536 between landscape metrics, long-term uplift and LGM ice thickness outlined above. The main  
537 difference between the domains north and south of the Rhône River is their lithology, and  
538 therefore their erodibility. Basins north of the Rhône are mainly underlain by lithologies of  
539 the Helvetic thrust nappes (erodibility classes 1-2) and the Aar massif (erodibility classes 3-  
540 4), while basins south of the Rhône are comprised of bedrock that is predominantly situated

541 in Penninic thrust nappes (erodibility classes 2-3). Indeed, topographic variables show quite  
542 strong variation in-between the three erodibility classes. Basins with low bedrock erodibility  
543 have higher elevation, relief and slope values than basins with a high erodibility. One factor  
544 influencing the erodibility of a rock is clearly the mechanical strength of the rocks, which has  
545 been inferred to be lower in carbonates than in granites or gneisses (Hoek & Brown, 1997;  
546 Kühni & Pfiffner, 2001). Rocks with a lower mechanical strength are eroded more easily in  
547 response to rainfall, runoff and mass movements (Norton et al., 2011; Cruz Nunes et al.,  
548 2015), which over a long time span can result in a lowering of elevation. Furthermore, slopes  
549 underlain by a mechanically weak material are more prone for failure than lithologies with  
550 greater strengths, particularly in transient landscapes as is the case here. It is possible that  
551 mechanically weaker lithotypes are not able to sustain high hillslope gradients over long  
552 periods of time (Kühni & Pfiffner, 2001)

553 Besides the mechanical rock strength itself, the susceptibility of the landscape towards  
554 erosion is also controlled by other factors including the structural fabric (faults, schistosity,  
555 bedding orientation) and seismicity (e.g. Persaud & Pfiffner, 2004; Molnar et al., 2007;  
556 Chittenden et al., 2014), as well as soil cover and potentials for mass movements like  
557 landslides (Norton et al., 2010a; Korup & Schlunegger, 2009; Cruz Nunes et al., 2015). There  
558 is a spatial clustering of earthquakes in the study area (figure 15), occurring most frequent  
559 northwest of the Rhône-Simplon-lineament in the area of the Helvetic nappes. Most  
560 earthquakes show a strike-slip focal mechanism and occur along steep-dipping ENE-WSW to  
561 WNW-ESE trending faults (Maurer et al. 1997). In the Penninic nappes south of the Rhône-  
562 Simplon-lineament, earthquakes show a wider spatial scatter and predominantly normal fault  
563 focal mechanisms. In contrast, earthquakes in the East of the study area occur more rarely,  
564 which coincides with the lack of large-scale tectonic faults (figure 15). Tonini et al. (2014)  
565 demonstrated that landslides are spatially clustered on the hillslopes bordering the Rhône  
566 valley and not in the tributary basins, and that gravitational slope deformations are likely  
567 coupled to earthquakes. Furthermore, they observed that landslides occur predominantly in  
568 unconsolidated Quaternary material (mainly glacial till), and that former landslide material is  
569 promoting new instabilities, thereby creating a positive feedback mechanism. Their map of  
570 landslides in the Rhône valley further shows a pattern similar to the distribution of faults,  
571 earthquakes and quaternary deposits (figure 15), all of which are being focused in the  
572 Helvetic nappes and near the lower elevations and valleys of the Penninic nappes.

573 Finally, the precipitation parameter is poorly correlated with any of the topographic  
574 characteristics. The only correlation between precipitation and landscape metrics has been

575 found for basins with very high precipitation rates, which appear to have generally high  
576 elevations, and also higher slope values. However, this is probably connected to the strong  
577 orographic effect in the Rhône basin (Frei and Schär, 1998). Basins that are characterized by  
578 higher elevations experience on average more (and also more intense) rainfall than the basins  
579 located in lower and therefore more shielded locations. In this context, the precipitation is  
580 rather the effect of than the cause for the high elevations. Therefore, the topographic variables  
581 can be assumed to be largely independent from climatic conditions such as precipitation  
582 (Schlunegger & Norton, 2013).

583

584 *Figure 15: Compiled map of faults (geological map of Switzerland 1:25000), earthquake*  
585 *epicentres (Swiss Earthquake catalogue) and landslides (Tonini et al., 2014). For reasons of*  
586 *clarity, we display only the earthquake epicentres of a short time period. For the full dataset*  
587 *and more detail about the data, see Fähr et al., 2011.*

588

## 589 **5. Conclusions**

590 We used standard topographic variables including mean elevation, relief, slope, hypsometry  
591 and river profile concavity to characterize the topography of the Rhône basin. A strong  
592 variation of these factors was observed between several sub-catchments. We therefore tested  
593 whether these differences can be explained by differences in uplift, glacial inheritance,  
594 precipitation conditions, or erodibility. From boxplots and linear discriminant function  
595 analysis we found that the variation of variables can best be explained using the affiliation of  
596 the basins with the general erodibility of the underlying bedrock. However, we also found  
597 correlations of some topographic variables with glacial inheritance and uplift. In particular,  
598 we showed that uplift could be responsible for the development of elevation and relief in the  
599 study area, whereas the ice thickness during the LGM influenced the elevation distribution  
600 (hypsometry) of the basins, as well as the shape of some of the river profiles. We conclude,  
601 therefore, that although the landscape shows evidence for pre-conditioning effects related to  
602 uplift and glaciation, the high spatial variation of bedrock erodibility offers the best  
603 explanation for the observed patterns of landscape form in the Rhône basin. In addition, the  
604 erodibility variable depends not only on the mechanical strength of the underlying bedrock,  
605 but also on the fault and earthquake densities, as well as the potential for landslides.

606 **Acknowledgements**

607 We would like to thank Romain Delunel for help during field work and river profile analysis.

608 We appreciated discussions with our project partners Maarten Bakker, Stéphanie Girardclos,

609 Stuart Lane, Jean-Luc Loizeau, Peter Molnar and Tiago Adriaio Silva. We thank the editors,

610 as well as J.D. Jansen and S. Brocklehurst for their careful and comprehensive reviews,

611 which greatly improved this manuscript.

612 This research was supported by the Swiss National Science Foundation (grant 147689).

613 **References**

- 614 Adams, J.: Contemporary uplift and erosion of the Southern Alps, New Zealand, Geological  
615 Society of America Bulletin, 91, 1-114, 1980.
- 616 Ahnert, F.: Local relief and the height limits of mountain ranges, American Journal of  
617 Science, 284, 1035-1055, 1984.
- 618 Baran, R., Friedrich, A.M. and Schlunegger, F.: The late Miocene to Holocene erosion  
619 pattern of the Alpine foreland basin reflects Eurasian slab unloading beneath the western  
620 Alps rather than global climate change, Lithosphere, 6, 124-131, 2014.
- 621 Bellin, N., Vanacker, V. and Kubik, P.W.: Denudation rates and tectonic geomorphology of  
622 the Spanish Betic Cordillera, Earth and Planetary Science Letters, 390, 19-30, 2014.
- 623 Bini, A., Buoncristani, J.-F., Couterrand, S., Ellwanger, D., Felber, M., Florineth, D., Graf,  
624 H.R., Keller, O., Kelly, M., Schlüchter, C., and Schoeneich P.: Switzerland during the last  
625 glacial maximum, Swisstopo, 1:500000, Wabern, 2009.
- 626 Brocklehurst, S.H. and Whipple, K.X.: Glacial erosion and relief production in the Eastern  
627 Sierra Nevada, California, Geomorphology, 42, 1-24, 2002.  
628
- 629 Brocklehurst, S.H. and Whipple, K.X.: Hypsometry of glaciated landscapes, Earth Surf.  
630 Process. Landforms, 29, 907–926, 2004.
- 631 Brozović, N., Burbank, D.W. and Meigs, A.J.: Climatic Limits on Landscape Development in  
632 the Northwestern Himalaya, Science, 276, 571-574, 1997.
- 633 Bull, W.B. and McFadden, L.D.: Tectonic geomorphology north and south of the Garlock  
634 fault, California. In: Doehering, D.O. (Ed.), Geomorphology in Arid Regions. Proceedings at  
635 the Eighth Annual Geomorphology Symposium, State University of New York, Binghamton,  
636 NY, 115-138, 1977.
- 637 Burbank, D.W., Leland, J., Fielding, E., Anderson, R.S., Brozović, N., Reid, M.R. and  
638 Duncan, C.: Bedrock incision, rock uplift and threshold hillslopes in the northwestern  
639 Himalayas, Nature, 379, 505-510, 1996.
- 640 Cederbom, C.E., van der Beek, P., Schlunegger, F., Sinclair, H.D., and Oncken, O.: Rapid  
641 extensive erosion of the North Alpine foreland basin at 5-4 Ma, Basin Research, 23, 528-550,  
642 2011.
- 643 Champagnac, J.-D., Molnar, P., Anderson, R.S., Sue, C., and Delacou, B.: Quarternary  
644 erosion-induced isostatic rebound in the western Alps, Geology, 35, 195-198, 2007.
- 645 Champagnac, J.-D., Schlunegger, F., Norton, K.P., von Blanckenburg, F., Abbühl, L.M., and  
646 Schwab, M.: Erosion-driven uplift of the modern Central Alps, Tectonophysics, 474, 236–  
647 249, 2009.
- 648 Cheng, K.-Y., Hung, J.-H., Chang, H.-C., Tsai, H., and Sung, Q.-C.: Scale independence of  
649 basin hypsometry and steady state topography, Geomorphology, 171-172, 1-11, 2012.

650 Chittenden, H., Delunel, R., Schlunegger, F., Akçar, N., and Kubik, P.: The influence of  
651 bedrock orientation on the landscape evolution, surface morphology and denudation ( $^{10}\text{Be}$ ) at  
652 the Niesen, Switzerland, *Earth Surface Processes and Landforms*, 39, 1153-1166, 2013.

653 Cruz Nunes, F., Delunel, R., Schlunegger, F., Akçar, N. and Kubik, P.: Bedrock bedding,  
654 landsliding and erosional budgets in the Central European Alps, *Terra Nova*, 00, 1-10, 2015.

655 Deichmann, N., Baer, M., Braunmiller, J., Ballarin Dolfin, D., Bay, F., Bernardi, F., Delouis,  
656 B., Fäh, D., Gerstenberger, M., Giardini, D., Huber, S., Kradofer, U., Maraini, S., Oprsal, I.,  
657 Schibler, R., Schler, T., Sellami, S., Steimen, S., Wiemer, S., Woessner, J. and Wyss, A.:  
658 Earthquakes in Switzerland and surrounding regions 2001, *Eclogae Geologicae Helveticae*, 95,  
659 249-262, 2002.

660 Dürst Stucki, M., Schlunegger, F., Christener, F., Otto, J.C. and Götz, J.: Deepening of inner  
661 gorges through subglacial meltwater - An example from the UNESCO Entlebuch area,  
662 Switzerland, *Geomorphology*, 139, 506-517, 2012.

663 Egli, D. and Mancktelow, N.: The structural history of the Mont Blanc massif with regard to  
664 models for its recent exhumation, *Swiss Journal for Geosciences*, 106, 469-489, 2013.

665 England, P. and Molnar, P.: Surface uplift, uplift of rocks, and exhumation of rocks, *Geology*,  
666 18, 1173-1177, 1990.

667 Fäh, D., Giardini, D., Kästli, P., Deichmann, N., Gisler, M., Schwarz-Zanetti, G., Alvarez-  
668 Rubio, S., Sellami, S., Edwards, B., Allmann, B., Bethmann, F., Wössner, J., Gassner-  
669 Stamm, G., Fritsche, S., and Eberhard, D.: ECOS-09 Earthquake Catalogue of Switzerland  
670 Release 2011 Report and Database, Public catalogue, Swiss Seismological Service ETH  
671 Zürich, Report SED/RISK/R/001/20110417, 2011.

672 Florineth, D. and Schlüchter, C.: Reconstructing the Last Glacial Maximum (LGM) ice  
673 surface geometry and flowlines in the Central Swiss Alps, *Eclogae Geologicae Helveticae*, 91,  
674 391-407, 1998.

675 Fox, M., Herman, F., Kissling, E. and Willett, S.D.: Rapid exhumation in the Western Alps  
676 driven by slab detachment and glacial erosion. *Geology*, 43, 379–382, 2015.

677 Frei C., and Schär, C.: A precipitation climatology of the Alps from high-resolution rain-gauge  
678 observations, *International Journal of Climatology*, 18, 873–900, 1998.

679 Froitzheim, N., Schmid, S.M. and Frey, M.: Mesozoic paleogeography and the timing of  
680 eclogite-facies metamorphism in the Alps: A working hypothesis, *Eclogae Geologicae  
681 Helveticae*, 89, 81–110, 1996.

682 Granger, D.E., Kirchner, J.W. and Finkel, R.: Spatially averaged long-term erosion rates  
683 measured from in situ-produced cosmogenic nuclides in alluvial sediment, *The Journal of  
684 Geology*, 104, 249-257, 1996.

685 Gudmundsson, G.: An order-of-magnitude estimate of the current uplift-rates in Switzerland  
686 caused by the Wurm Alpine deglaciation, *Eclogae Geologicae Helveticae*, 87, 545-557, 1994

687 Hack, J. T.: Studies of longitudinal stream profiles in Virginia and Maryland, U.S. Geological  
688 Survey Professional Paper, 294-B, 1957.

- 689 Hallett, B., Hunter, L., and Bogen, J.: Rates of erosion and sediment evacuation by glaciers:  
690 A review of field data and their implications, *Global and Planetary Change*, 12, 213-235,  
691 1996.
- 692 Hergarten, S., Wagner, T., and Stüwe, K.: Age and prematurity of the Alps derived from  
693 topography, *Earth and Planetary Science Letters*, 297, 453-460, 2010.
- 694 Hoek, E. and Brown, E.T.: Practical estimates of rock mass strength, *International Journal of*  
695 *rock mechanics and mining sciences*, 34, 1165-1186, 1997.
- 696 Hurtrez, J.-E., Lucazeau, F., Lavé, J., and Avouac, J.-P.: Investigation of the relationships  
697 between basin morphology, tectonic uplift, and denudation from the study of an active fold  
698 belt in the Siwalik hills, central Nepal, *Journal of Geophysical research*, 104, 12779-12796,  
699 1999.
- 700 Ivy-Ochs, S., Kreschner, H., Reuther, A., Preusser, F., Heine, K., Maisch, M., Kubik, P.W.,  
701 Schlüchter, C.: Chronology of the last glacial cycle in the European Alps, *Journal of*  
702 *Quaternary Science*, 23, 559-573, 2008.
- 703 Jäckli, H.: *Gegenwartsgeologie des bündnerischen Rheingebietes. Beitr. Geol. Schweiz.* 36,  
704 136 p., 1957.
- 705 Jansen, J.D., Codilean, A.T., Stroeve, A.P., Fabel, D., Hättestrand, C., Kleman, J., Harbor,  
706 J.M., Heyman, J., Kubik, P.W. and Xu, S.: Inner gorges cut by subglacial meltwater during  
707 Fennoscandian ice sheet decay, *Nature communications*, 5, 3815, 2014,  
708 doi:10.1038/ncomms4815
- 709 Kahle, H.G., Geiger, A., Bürki, B., Gubler, E., Marti, U., Wirth, B., Rothacher, M., Gurtner,  
710 W., Beutler, G., Bauersima, I. and Pfiffner, O.A.: Recent crustal movements, geoid and  
711 density distribution: Contribution from integrated satellite and terrestrial measurements, In:  
712 Pfiffner, O.A., Lehner, P., Heitzmann, P., Müller, S. and Steck, A. (Eds.), *Deep structure of*  
713 *the Swiss Alps: Results of NRP 20*, Birkhäuser Verlag, Basel, 251-259, 1997.
- 714 Kelly, M.A., Buoncristiani, J.F., and Schlüchter, C.: A reconstruction of the last glacial  
715 maximum (LGM) ice-surface geometry in the western Swiss Alps and contiguous Alpine  
716 regions in Italy and France, *Eclogae Geologicae Helvetiae*, v. 97, 57-75, 2004.
- 717 Korup, O.: Rock type leaves topographic signature in landslide-dominated mountain ranges,  
718 *Geophysical Research Letters*, 35, L11402, doi:10.1029/2008GL034157, 2008.
- 719 Korup, O. and Montgomery, D.R.: Tibetan plateau river incision inhibited by glacial  
720 stabilization of the Tsangpo gorge, *Nature*, 455, 786-790, 2008.
- 721 Korup, O., and Schlunegger, F.: Bedrock landsliding, river incision, and transience of  
722 geomorphic hillslope-channel coupling: Evidence from inner gorges in the Swiss Alps,  
723 *Journal of Geophysical Research*, 112, F03027, doi:10.1029/2006JF000710, 2007.
- 724 Korup, O., and Schlunegger, F.: Rock-type control on erosion-induced uplift, eastern Swiss  
725 Alps, *Earth and Planetary Science Letters*, 278, 278-285, 2009.
- 726 Korup, O., and Weidinger, J.T.: Rock type, precipitation, and the steepness of Himalayan  
727 threshold hillslopes, *Geological Society, London, Special Publications*, 353, 235-249, 2011



- 728 Korup, O., Schmidt, J., and McSaveney, M.J.: Regional relief characteristics and denudation  
729 pattern of the western Southern Alps, New Zealand, *Geomorphology*, 71, 402-423, 2005.
- 730 Kuhlemann, J., Frisch, W., Székely, B., Dunkl, I., and Kázmér, M.: Post-collisional sediment  
731 budget history of the Alps: tectonic versus climatic control, *International Journal of Earth  
732 Sciences*, 91, 818-837, 2002.
- 733 Kühni, A. and Pfiffner, O.A.: The relief of the Swiss Alps and adjacent areas and its relation  
734 to lithology and structure: topographic analysis from a 250-m DEM, *Geomorphology*, 41,  
735 285-307, 2001.
- 736 Lyon-Caen, H., and Molnar, P.: Constraints on the deep structure and dynamic processes  
737 beneath the Alps and adjacent regions from an analysis of gravity anomalies, *Geophysical  
738 Journal International*, 99, 19–32, 1989.
- 739 Maurer, H.R., Burkhard, M, Deichmann, N. and Green, A.G.: Active tectonism in the central  
740 Alps: contrasting stress regimes north and south of the Rhone Valley, *Terra Nova*, 9, 91-94,  
741 1997.
- 742 McLachlan, G.J.: *Discriminant analysis and statistical pattern recognition*. Wiley  
743 Interscience, New York, 552 p., 2004.
- 744 Michalski, I., and Soom, M.: The Alpine thermo-tectonic evolution of the Aar and Gotthard  
745 massifs, Central Switzerland: Fission Track ages on zircon and apatite and K-Ar mica ages,  
746 *Schweizerische mineralogische und petrographische Mitteilungen*, 70, 373-388, 1990.
- 747 Molnar, P. Anderson, R.S., and Anderson, S.P., *Tectonics, fracturing of rock, and erosion*,  
748 *Journal of Geophysical Research*, 112, F03014, doi:10.1029/2005JF000433, 2007.  
749
- 750 Montgomery, D.R. and Brandon, M.T.: Topographic controls on erosion rates in tectonically  
751 active mountain ranges, *Earth and Planetary Science Letters*, 201, 481-489, 2002.
- 752 Montgomery, D.R.: Valley formation by fluvial and glacial erosion, *Geology*, 30, 1047-1050,  
753 2002.
- 754 Montgomery, D.R., Balco, G. and Willett, S.D.: Climate, tectonics, and the morphology of  
755 the Andes, *Geology*, 29, 579–582, 2001.
- 756 Morel, P., von Blanckenburg, F., Schaller, M., Kubik, P.W., and Hinderer, M.: Lithology,  
757 landscape dissection and glaciation controls on catchment erosion as determined by  
758 cosmogenic nuclides in river sediment (the Wutach Gorge, Black Forest), *Terra Nova*, 15,  
759 398-404, 2003.
- 760 Niggli, P., and de Quervain, F.D.: *Geotechnische Karte der Schweiz*. Schweizerische  
761 Geotechnische Kommission, Kümmerly and Frey, Geotechnischer Verlag, Bern, 1936.
- 762 Norton, K.P., von Blanckenburg, F., Schlunegger, F., Schwab, M., and Kubik, P.W.:  
763 Cosmogenic nuclide-based investigation of spatial erosion and hillslope channel coupling in  
764 the transient foreland of the Swiss Alps, *Geomorphology*, 95, 474-486, 2008.
- 765 Norton, K.P., von Blanckenburg, F. and Kubik, P.W.: Cosmogenic nuclide-derived rates of  
766 diffusive and episodic erosion in the glacially sculpted upper Rhone Valley, Swiss Alps,  
767 *Earth Surface Processes and Landforms*, 35, 651–662, 2010a.

768 Norton, K.P., Abbühl, L.M. and Schlunegger, F.: Glacial conditioning as an erosional driving  
769 force in the Central Alps, *Geology*, 38, 655-658, 2010b.

770 Norton, K.P., von Blanckenburg, F., DiBiase, R., Schlunegger, F., and Kubik, P.W.:  
771 Cosmogenic <sup>10</sup>Be-derived denudation rates of the Eastern and Southern European Alps,  
772 *International Journal of Earth Sciences*, 100, 1163-1179, 2011.

773 Ouimet, W.B., Whipple, K.X., and Granger, D.E.: Beyond threshold hillslopes: Channel  
774 adjustment to base-level fall in tectonically active mountain ranges, *Geology*, 37, 579-582,  
775 2009.

776 Pérez-Peña, J.V., Azor, A., Azañón, J.M., and Keller, E.A.: Active tectonics in the Sierra  
777 Nevada (Betic Cordillera, SE Spain): Insights from geomorphic indexes and drainage pattern  
778 analysis, *Geomorphology*, 119, 74-87, 2010.

779 Persaud, M. and Pfiffner, O.A.: Active deformation in the eastern Swiss Alps: post-glacial  
780 faults, seismicity and surface uplift, *Tectonophysics*, 385, 59-84, 2004.

781 Pfiffner, O.A., Sahli, S., Stäubli, M.: Compression and uplift of the external massifs in the  
782 Helvetic zone, In: Pfiffner, O.A., Lehner, P., Heitzmann, P., Müller, S. and Steck, A. (Eds.),  
783 *Deep Structure of the Swiss Alps: Results of NRP 20*, Birkhäuser, Switzerland, 139–153,  
784 1997.

785 Robl, J., Prasicek, G., Hergarten, S., and Stüwe, K.: Alpine topography in the light of tectonic  
786 uplift and glaciation, *Global and Planetary Change*, 127, 34-49, 2015.

787 Schaller, M., von Blanckenburg, F., Hovius, N., and Kubik, P.W.: Large-scale erosion rates  
788 from in situ-produced cosmogenic nuclides in European river sediments, *Earth and Planetary  
789 Science Letters*, 188, 441-458, 2001.

790 Scharf, T. E., Codilean, A. T., De Wit, M., Jansen, J. D., and Kubik, P. W.: Strong rocks  
791 sustain ancient postorogenic topography in southern Africa. *Geology*, 41, 331-334, 2013.

792 Schlatter, A., Schneider, D., Geiger, A., and Kahle, H.G.: Recent vertical movements from  
793 precise levelling in the vicinity of the city of Basel, Switzerland, *International Journal of  
794 Earth Sciences*, 94, 507–514, 2005.

795 Schlunegger, F. and Hinderer, M.: Crustal uplift in the Alps: why the drainage pattern  
796 matters, *Terra Nova*, 13, 425-432, 2001.

797 Schlunegger, F. and Norton, K.P.: Water versus ice: The competing roles of modern climate  
798 and Pleistocene glacial erosion in the Central Alps of Switzerland, *Tectonophysics*, 602, 370-  
799 381, 2013.

800 Schlunegger, F. and Willett, S.D.: Spatial and temporal variations in exhumation of the  
801 Central Swiss Alps and implications for exhumation mechanisms, In: Ring, U., Brandon,  
802 M.T., Lister, G.S. and Willett, S.D. (Eds.), *Exhumation processes: normal faulting, ductile  
803 flow, and erosion: Geological Society of London Special Publication 154*, 157-180, 1999.

804 Schlunegger, F., Melzer, J. and Tucker, G.E.: Climate, exposed source-rock lithologies,  
805 crustal uplift and surface erosion: a theoretical analysis calibrated with data from the

- 806 Alps/North Alpine Foreland Basin system, *International Journal of Earth Sciences*, 90, 484–  
807 499, 2001.
- 808 Schlunegger, F., Badoux, A., McArdell, B.W., Gwerder, C., Schnydrig, D., Rieke-Zapp, D.  
809 and Molnar, P.: Limits of sediment transfer in an alpine debris-flow catchment, Illgraben,  
810 Switzerland, *Quaternary Science Reviews*, 28, 1097–1105, 2009.
- 811 Schmid, S.M., Pfiffner, O.A., Froitzheim, N., Schönborn, G., and Kissling, E.: Geophysical-  
812 geological transect and tectonic evolution of the Swiss-Italian Alps, *Tectonics*, 15, 1036–  
813 1064, 1996.
- 814 Schmid, S.M., Fügenschuh, B., Kissling, E. and Schuster, R., *Tectonic map and overall*  
815 *architecture of the Alpine orogen*, *Eclogae Geologicae Helveticae*, v. 97, p. 93–117, 2004.
- 816 Schmidt, K.M. and Montgomery, D.R., *Limits to Relief*, *Science*, 270, 617-620, 1995.
- 817 Schwarb, M.: *The Alpine Precipitation Climate Evaluation of a High-Resolution Analysis*  
818 *Scheme using Comprehensive Rain-Gauge Data*, Ph.D. thesis, ETH Zurich, Switzerland,  
819 2000.
- 820 Seward, D. and Mancktelow, N.S.: Neogene kinematics of the central and western Alps:  
821 Evidence from fission-track dating, *Geology*, 22, 803-806, 1994.
- 822 Shuster, D.L., Ehlers, T.A., Rusmore, M.E., Farley, K.A.: Rapid glacial erosion at 1.8 Ma  
823 revealed by  $^4\text{He}/^3\text{He}$  thermochronology, *Science*, 310, 1668-1670, 2005.
- 824 Small, E.E., and Anderson, R.S.: Pleistocene relief production in Laramide mountain ranges,  
825 western United States, *Geology*, 26, 123–126, 1998.
- 826 Snyder, N.P., Whipple, K.X., Tucker, G.E., and Merritts, D.J.: Landscape response to  
827 tectonic forcing: DEM analysis of stream profiles in the Mendocino triple junction region,  
828 northern California, *Geological Society of America Bulletin*, 112, no. 8, 1250–1263, 2000.
- 829 Snyder, N.P., Whipple, K.X, Tucker, G.E., and Merritts, D.J.: Channel response to tectonic  
830 forcing: Field analysis of stream morphology and hydrology in the Mendocino triple junction  
831 region, northern California, *Geomorphology*, 53, 97–127, 2003
- 832 Spotila, J.A., Buscher, J.T., Meigs, A.J., and Reiners, P.W.: Long-term glacial erosion of  
833 active mountain belts: Example of the Chugach-St. Elias Range, Alaska, *Geology*, 32, 501-  
834 504, 2004.
- 835 Strahler, A.N.: Hypsometric (area-altitude) analysis of erosional topography, *Bulletin of the*  
836 *Geological Society of America*, 63, 1117-1142, 1952.
- 837 Stüwe, K., White, L., and Brown, R.: The influence of eroding topography on steady-state  
838 isotherms. Application to fission track analysis, *Earth and Planetary Science Letters*, 124, 63-  
839 74, 1994.
- 840 Sue, C., Delacou, B., Champagnac, J.-D., Allanic, C., Tricart, P., and Burkhard, M.:  
841 Extensional neotectonics around the bend of the western/central Alps: An overview,  
842 *International Journal of Earth Sciences*, 96, 1101–1129, 2007.

- 843 Tonini, M., Pedrazzini, A., Penna, I., and Jaboyedoff, M.: Spatial pattern of landslides in  
844 Swiss Rhone Valley, *Natural Hazards*, 73, 97-110, 2014.
- 845 Ustaszewski, M., Herwegh, M., McClymont, A.F., Pfiffner, O.A., Pickering, R. and Preusser,  
846 F.: Unravelling the evolution of an Alpine to post-glacially active fault in the Swiss Alps,  
847 *Journal of Structural Geology*, 29, 1943-1959, 2007.
- 848 Valla, P.G., Shuster, D.L., and van der Beek, P.: Significant increase in relief of the European  
849 Alps during mid-Pleistocene glaciations, *Nature Geosciences*, 4, 688-692, 2011.
- 850 Vernon, A.J., van der Beek, P.A., Sinclair, H.D., Rahn, M.K.: Increase in late Neogene  
851 denudation of the European Alps confirmed by analysis of a fission-track thermochronology  
852 database, *Earth and Planetary Science Letters*, 270, 316-329, 2008.
- 853 Whipple, K.X.: Bedrock rivers and the geomorphology of active orogens, *Annual Review of*  
854 *Earth and Planetary Science*, 32, 151–185, 2004.
- 855 Whipple, K.X., and Tucker, G.E.: Dynamics of the stream-power river incision model:  
856 Implications for the height limits of mountain ranges, landscape response time scales, and  
857 research needs, *Journal of Geophysical Research*, 104, no. B8, 17661–17674, 1999.
- 858 Willett, S.D.: Orogeny and orography: The effects of erosion on the structure of mountain  
859 belts, *Journal of Geophysical Research*, 104, 28957-28981, 1999.
- 860 Willett, S.D., and Brandon, M.T.: On steady states in mountain belts, *Geology*, 30, 175-178,  
861 2002.
- 862 Willett, S.D., Schlunegger, F. and Picotti, V.: Messinian climate change and erosional  
863 destruction of the central European Alps, *Geology*, 34, 613-616, 2006.
- 864 Willett, S.D., McCoy, S.W., Perron, T., Goren, L. and Chen, C.: Dynamic reorganization of  
865 river basins, *Science*, 343, 1248765, 2014.
- 866 Willgoose, G. and Hancock, G.: Revisiting the hypsometric curve as an indicator of form and  
867 process in transport-limited catchment, *Earth Surface Processes and Landforms*, 23, 611–623,  
868 1998.
- 869 Wittmann, H., von Blanckenburg, F., Kruesmann, T., Norton, K.P., and Kubik, P.W.:  
870 Relation between rock uplift and denudation from cosmogenic nuclides in river sediment in  
871 the Central Alps of Switzerland, *Journal of Geophysical Research*, 112, F04010, 2007,  
872 doi:10.1029/2006JF000729
- 873 Wobus, C., Whipple, K.X, Kirby, E., Snyder, E., Johnson, J., Spyropolou, K., Crosby, B., and  
874 Sheehan, D.: Tectonics from topography: Procedures, promise, and pitfalls, In: Willett, S.D.,  
875 Hovius, N., Brandon, M.T. and Fisher, D.M. (Eds.), *Tectonics, climate, and landscape*  
876 *evolution: Geological Society of America Special Paper*, Boulder, Colorado, USA, 398, 55–  
877 74, 2006.

878 Table 1

Catchment	Catchment size (km <sup>2</sup> )	Mean elevation (m)	Local relief (m)	Slope (°)	HI	k <sub>s</sub>	θ
Aegene	36.0	2420.2	641.2	29.8	0.37	0.57	0.18
Avancon	82.6	1676.6	747.7	29.8	0.36	4.05	0.32
Baltschiederbach	42.6	2395.3	949.9	38.4	0.44	0.58	0.11
Bietschbach	21.9	2273.1	973.5	39.0	0.45	3.21	0.29
Binna	116.1	2215.9	729.8	31.0	0.47	16.72	0.31
Blinne	18.3	2371.5	831.5	36.6	0.39	7.85	0.54
Borgne	385.1	2399.1	798.0	30.3	0.44	3.24	0.27
Boverече	18.6	1732.1	609.5	23.9	0.42	8.56	0.40
Chelchbach	27.1	2112.1	711.5	26.6	0.45	1.24	0.19
Dala	58.5	2036.4	860.5	31.7	0.42	4.48	0.29
Dranse	674.8	2243.7	836.8	31.6	0.35	1.97	0.26
Farne	29.0	1846.8	712.5	28.7	0.42	1.81	0.24
Feschilju	18.1	2133.0	683.5	28.6	0.51	0.13	-0.05
Fossau	11.7	1373.0	717.8	33.3	0.50	0.10	-0.04
Fully	10.4	2149.9	828.6	29.2	0.57	0.00	-0.53
Gamsa	38.5	2199.7	739.8	30.5	0.49	0.25	0.04
Goneri	40.0	2371.9	732.9	31.8	0.43	2.05	0.30
GrandEau	130.0	1570.4	682.9	26.6	0.29	57.95	0.55
Grefe	10.5	1429.3	641.6	27.7	0.59	0.00	-0.83
Gryonne	34.8	1423.4	471.1	21.7	0.48	0.08	0.01
Illbach	11.0	1816.8	833.0	37.6	0.33	15.06	0.82
Jolibach	11.5	2288.8	882.5	36.2	0.51	0.25	-0.02
Liene	92.3	1910.0	608.2	25.4	0.40	1.43	0.24
Lixerne	64.8	1920.2	843.7	33.1	0.43	1.24	0.21
Lonza	161.5	2361.2	871.5	33.3	0.46	6.09	0.28
Losentse	22.1	1618.0	838.7	33.3	0.33	13.94	0.58
Massa	202.9	2891.1	712.6	36.4	0.64	0.00	-0.18
Milibach2	15.9	2236.5	600.7	20.6	0.54	0.01	-0.22
Morge	72.1	1823.5	598.5	26.4	0.42	1.45	0.21
Mundbach	23.8	2305.8	991.0	40.7	0.50	0.56	0.06
Münstigerbach	15.7	2455.7	743.3	33.1	0.34	143.34	0.59
Navisence	255.8	2389.8	790.9	30.2	0.51	4.42	0.31
Printse	72.1	2137.8	659.2	27.6	0.50	0.09	-0.02
Randonne	11.9	2124.1	749.3	31.5	0.67	0.00	-1.32
Raspille	27.6	2158.4	614.9	27.1	0.49	0.17	0.00
Reche	26.9	2124.9	687.6	27.1	0.53	0.01	-0.21
Salanfe	25.9	2139.4	849.6	30.0	0.70	0.00	-2.69
Salantse	19.9	1804.1	704.9	29.7	0.48	0.53	0.10
Saltina	76.8	2008.3	776.8	30.9	0.39	3.65	0.31
Sionne	26.7	1578.9	561.7	19.6	0.35	8.57	0.54
Torgon	11.2	1441.8	539.2	27.7	0.58	0.00	-0.40
T. St. Barthelemy	12.4	1705.5	948.9	26.6	0.34	57.75	0.66
Tove	12.3	1604.9	697.9	31.6	0.60	0.00	-0.71
Trient	83.2	1898.5	832.6	34.4	0.37	57.93	0.63
Turtmanna	108.0	2512.7	725.0	29.8	0.59	1.17	0.15
Viexe	134.8	1651.2	731.2	28.3	0.30	385.20	0.56
Vispa	773.9	2640.8	867.3	32.4	0.32	42.41	0.41
Walibach	12.1	2524.1	773.2	31.6	0.47	1.44	0.19
Wysswasser	84.6	2636.1	727.3	33.8	0.28	0.08	-0.02

Yvorne	10.2	1307.3	744.7	27.1	0.49	0.13	-0.01
--------	------	--------	-------	------	------	------	-------

879 Table 2

Catchment	Apatite-FT ages (My)	Recent uplift rate (mm/y)	LGM ice thickness (m)	Mean annual precipitation (mm/y)	Annual 90 <sup>th</sup> percentile (mm/d)	Erodibility
Aegene	5.0	1.23	482	2018.0	29.77	2.34
Avancon	8.1	0.67	339	1839.8	28.73	1.78
Baltschiederbach	3.1	1.54	421	1325.4	27.80	3.92
Bietschbach	2.9	1.50	445	1301.7	25.91	3.28
Binna	4.8	1.48	475	1446.7	27.00	2.56
Blinne	5.0	1.37	415	2010.4	32.52	2.14
Borgne	8.9	1.26	281	1097.5	19.95	3.31
Bovereche	5.9	1.39	567	1269.4	25.55	1.82
Chelchbach	3.3	1.51	611	1198.7	30.01	3.99
Dala	3.8	1.28	438	1581.4	28.22	2.00
Dranse	7.1	1.01	364	1332.8	22.42	2.73
Farne	8.0	1.03	275	976.2	19.09	2.09
Feschilju	3.0	1.36	309	1542.7	28.46	2.47
Fossau	8	0.38	348	1794.5	28.46	2.00
Fully	3.8	0.72	164	1663.2	28.49	2.77
Gamsa	3.7	1.36	433	1318.4	25.49	2.89
Goneri	5.0	1.08	591	2104.6	28.47	3.74
GrandEau	11.5	0.58	292	1675.1	25.26	1.36
Greffe	6.8	0.46	247	1761.4	27.47	1.98
Gryonne	10.8	0.59	344	1521.2	23.61	1.17
Illbach	6.7	1.41	467	1114.2	21.00	1.91
Jolibach	3.0	1.49	367	1258.8	24.92	2.99
Liene	6.2	1.32	396	1433.5	26.60	1.83
Lixerne	6.0	0.93	321	1802.7	30.90	2.00
Lonza	3.8	1.34	424	1507.1	25.31	3.13
Losentse	5.1	0.85	517	1292.5	22.86	2.00
Massa	4.9	1.37	258	2266.7	37.68	3.65
Milibach2	5.0	1.47	423	1557.3	28.20	1.86
Morge	5.9	1.15	417	1734.3	30.75	1.98
Mundbach	3.2	1.54	476	1387.1	31.64	3.99
Münstigerbach	5.0	1.21	413	1940.9	29.93	3.99
Navisence	8.0	1.34	306	1118.6	21.47	3.02
Printse	9.7	1.20	235	1028.6	19.73	2.86
Randonne	5.0	0.74	113	1797.6	30.05	2.47
Raspille	5.0	1.31	389	1667.2	29.83	1.91
Reche	8.9	1.55	194	1011.9	19.75	2.96
Salanfe	3.6	0.65	142	1823.6	30.33	2.83
Salantse	5.0	0.77	273	1610.8	26.90	2.02
Saltina	3.0	1.45	651	1325.7	24.94	2.65
Sionne	6.1	1.34	581	1278.5	25.21	1.73
Torgon	8	0.4	209	1752.8	27.64	2.00
T. St. Barthelemy	4.1	0.62	284	1665.1	27.75	2.49
Tove	8	0.3	217	2009.8	31.83	2.00
Trient	4.1	0.81	396	1559.3	27.32	3.34
Turtmanna	6.9	1.34	243	1102.6	21.76	3.14
Viexe	5.0	0.50	307	1709.2	26.86	1.64
Vispa	6.8	1.10	411	1242.4	25.44	3.20
Walibach	5.0	1.33	314	1983.7	34.97	3.98

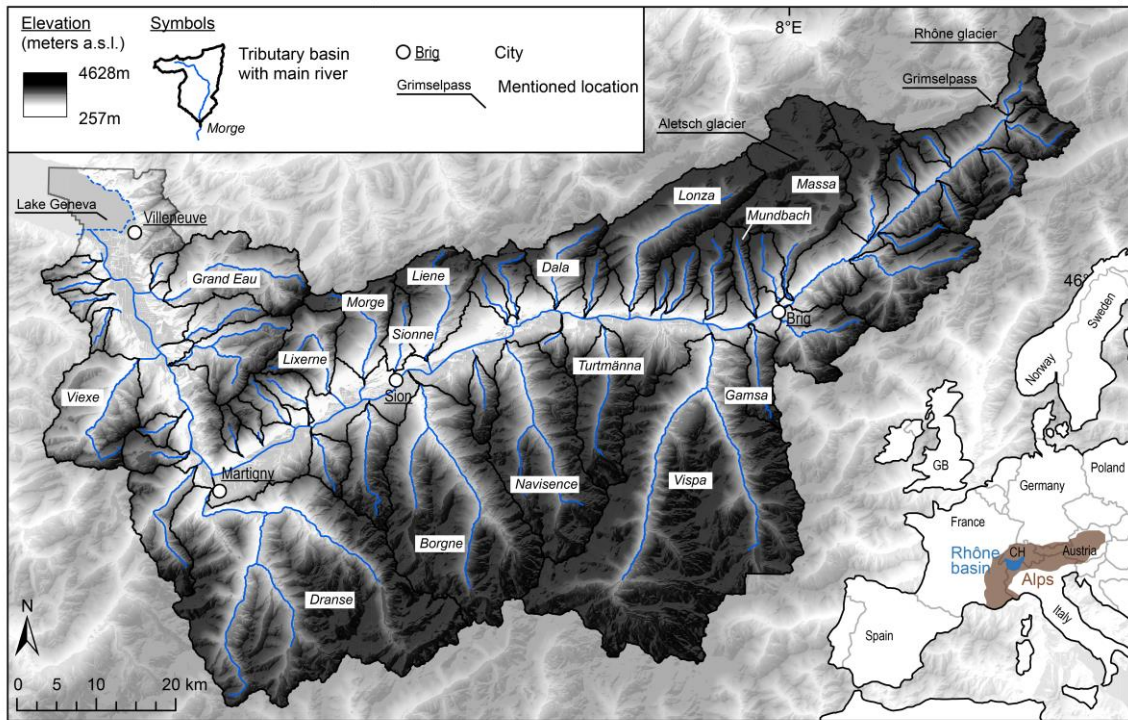
Wysswasser	5.0	1.34	403	2136.3	37.95	3.92
Yvorne	11.8	0.4	389	1388.8	22.17	2.00



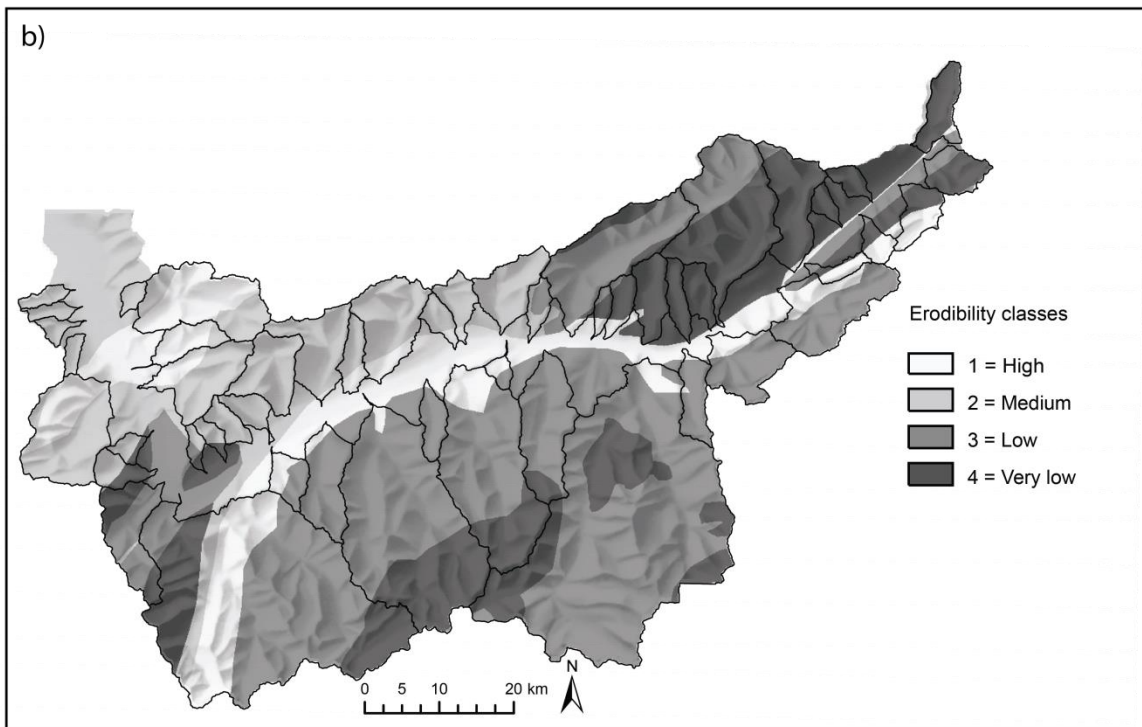
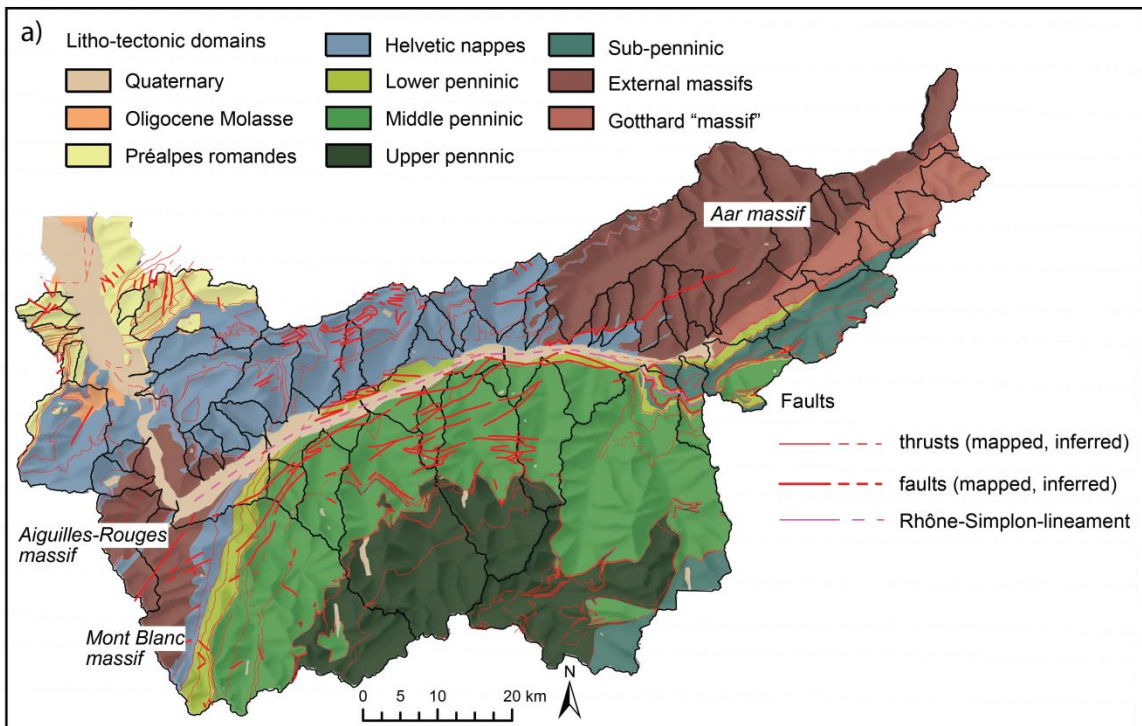
Uplift (long-term), in My					
Class	Classified as 1	Classified as 2	Classified as 3	Correctly classified	Total correct classification
1 (1.5-5.0)	9	5	0	64.29%	66%
2 (5.0-8.0)	3	19	2	79.17%	
3 (8.0-12.0)	1	6	5	41.67%	
Uplift (short-term), in mm/y					
Class	Classified as 1	Classified as 2	Classified as 3	Correctly classified	Total correct classification
1 (0.5-0.9)	19	2	1	86.36%	76%
2 (0.9-1.4)	3	15	1	78.95%	
3 (1.4 – 1.6)	1	4	4	44.44%	
LGM ice thickness, in m					
Class	Classified as 1	Classified as 2	Classified as 3	Correctly classified	Total correct classification
1 (113-292)	8	7	0	53.33%	62%
2 (292-471)	3	23	0	88.46%	
3 (471-651)	0	9	0	0%	
Amount of precipitation (mean annual, in mm/y)					
Class	Classified as 1	Classified as 2	Classified as 3	Correctly classified	Total correct classification
1 (975-1340)	14	6	9	70.00%	70%
2 (1340-1840)	6	15	0	71.43%	
3 (1840-2278)	1	2	6	66.67%	
Intensity of precipitation (90 <sup>th</sup> percentile, in mm/day)					
Class	Classified as 1	Classified as 2	Classified as 3	Correctly classified	Total correct classification
1 (19-25)	2	11	0	15.38%	74%
2 (25-31)	0	31	0	100%	
3 (31-37)	0	2	4	66.67%	
Erodibility					
Class	Classified as 1	Classified as 2	Classified as 3	Correctly classified	Total correct classification
1 (1-2, high)	17	4	0	80.95%	80%
2 (2-3, medium)	0	11	4	73.33%	

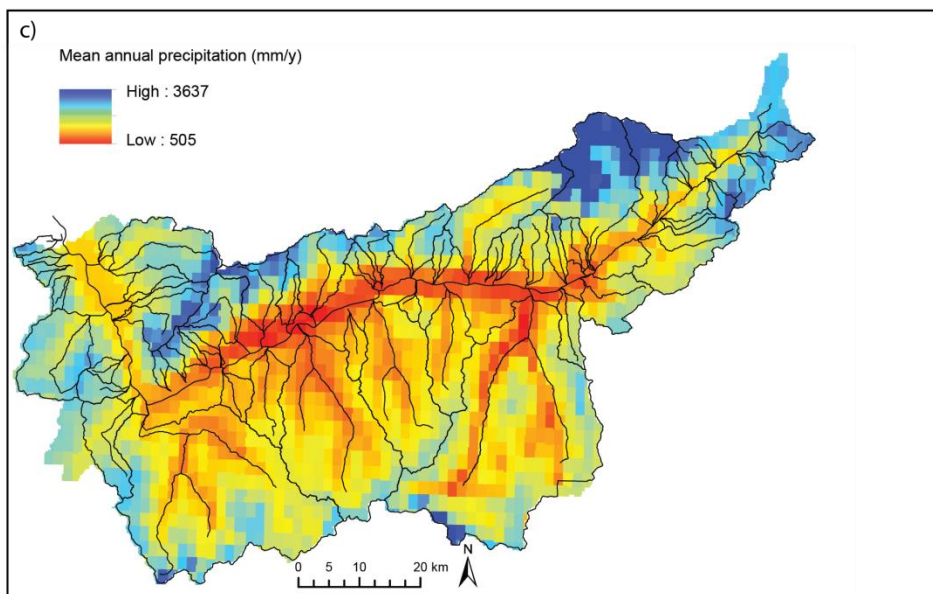
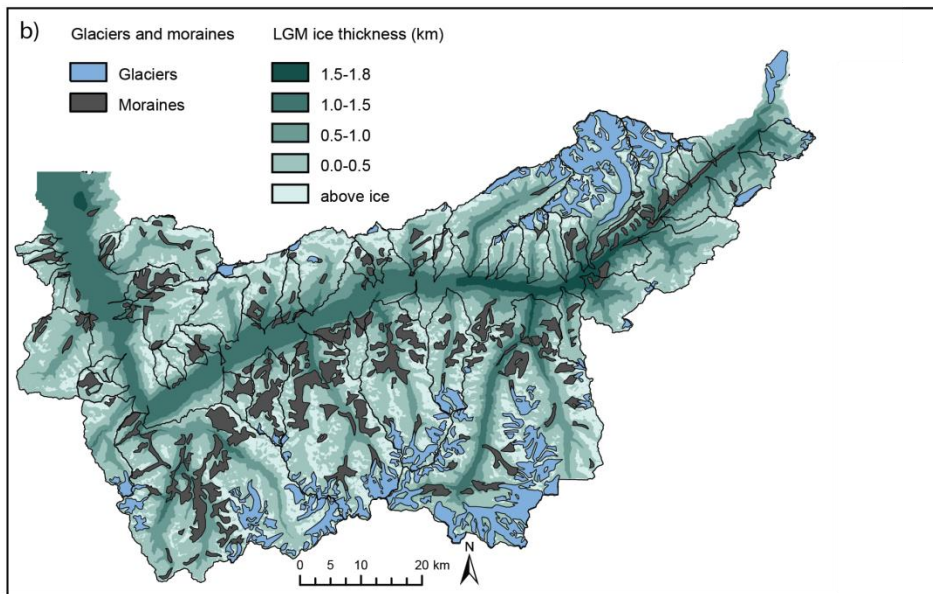
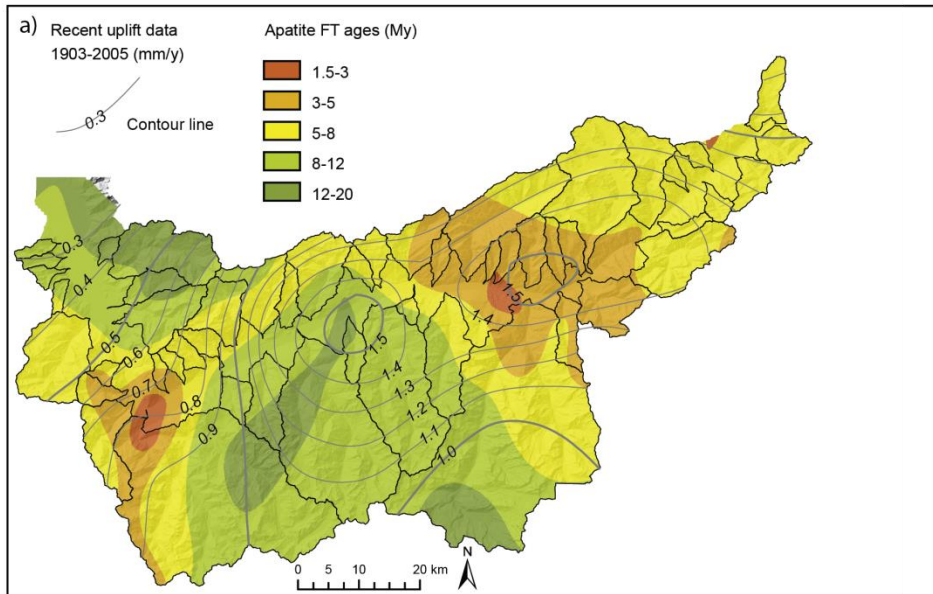
3 (3-4, low)	1	1	12	85.71%	
--------------	---	---	----	--------	--

881 Figure 1

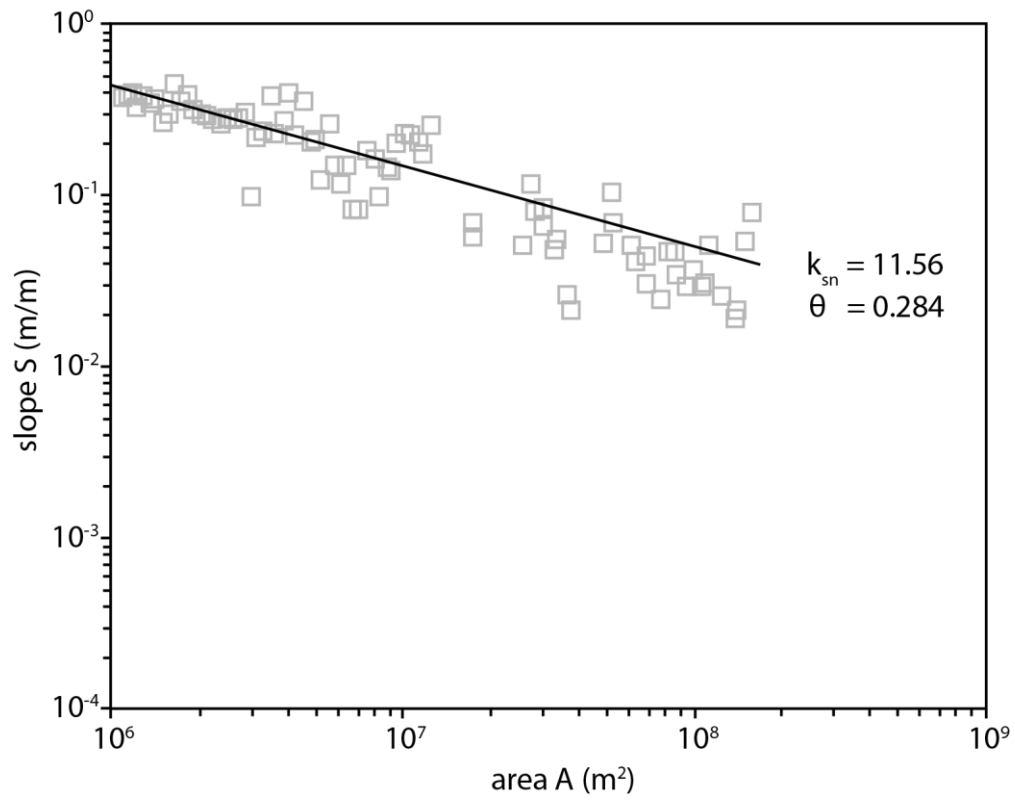


882



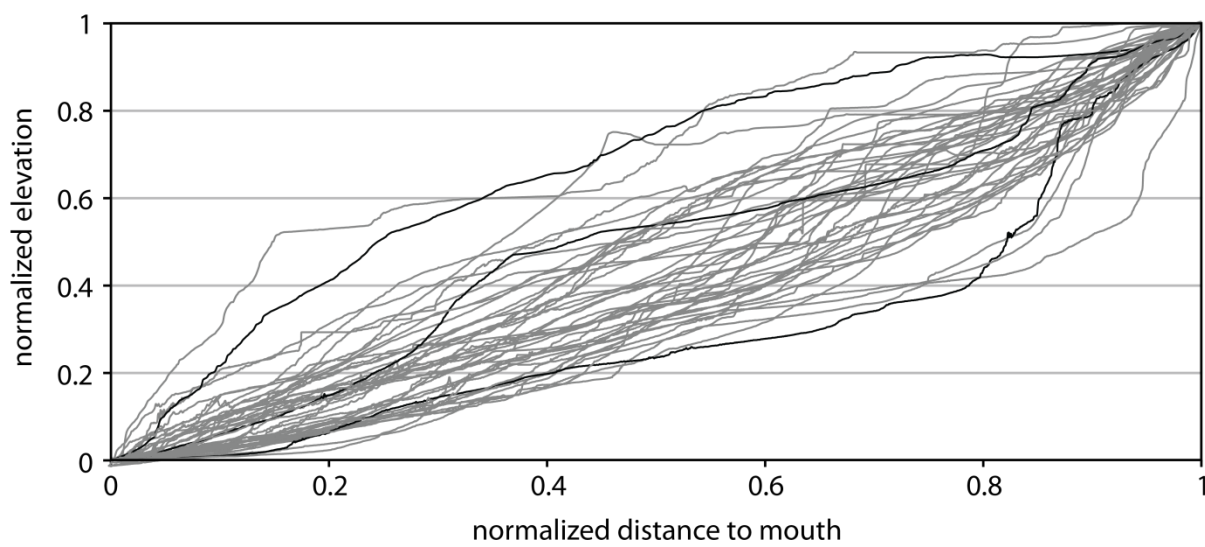


886 Figure 4



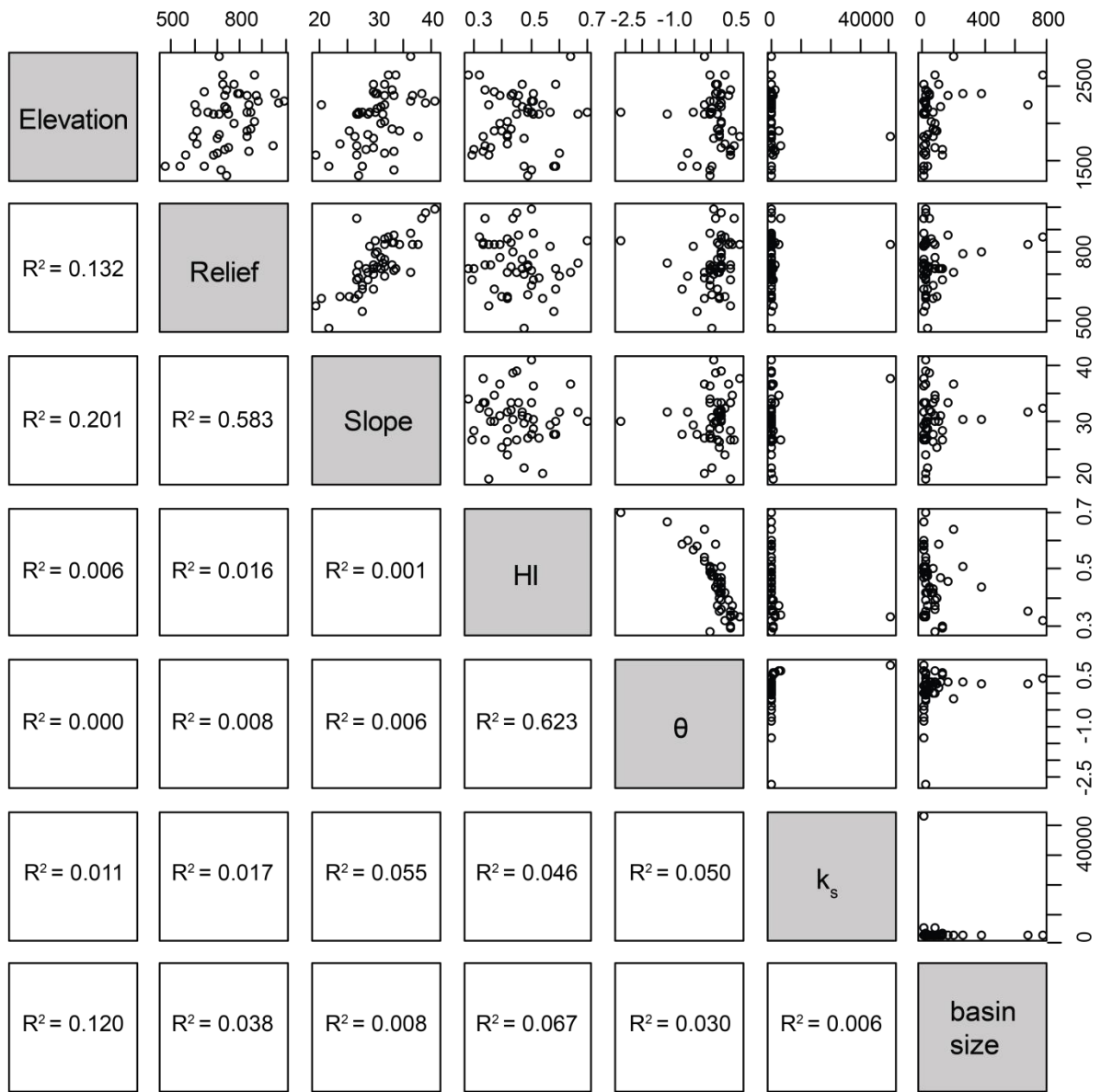
887

888 Figure 5



889

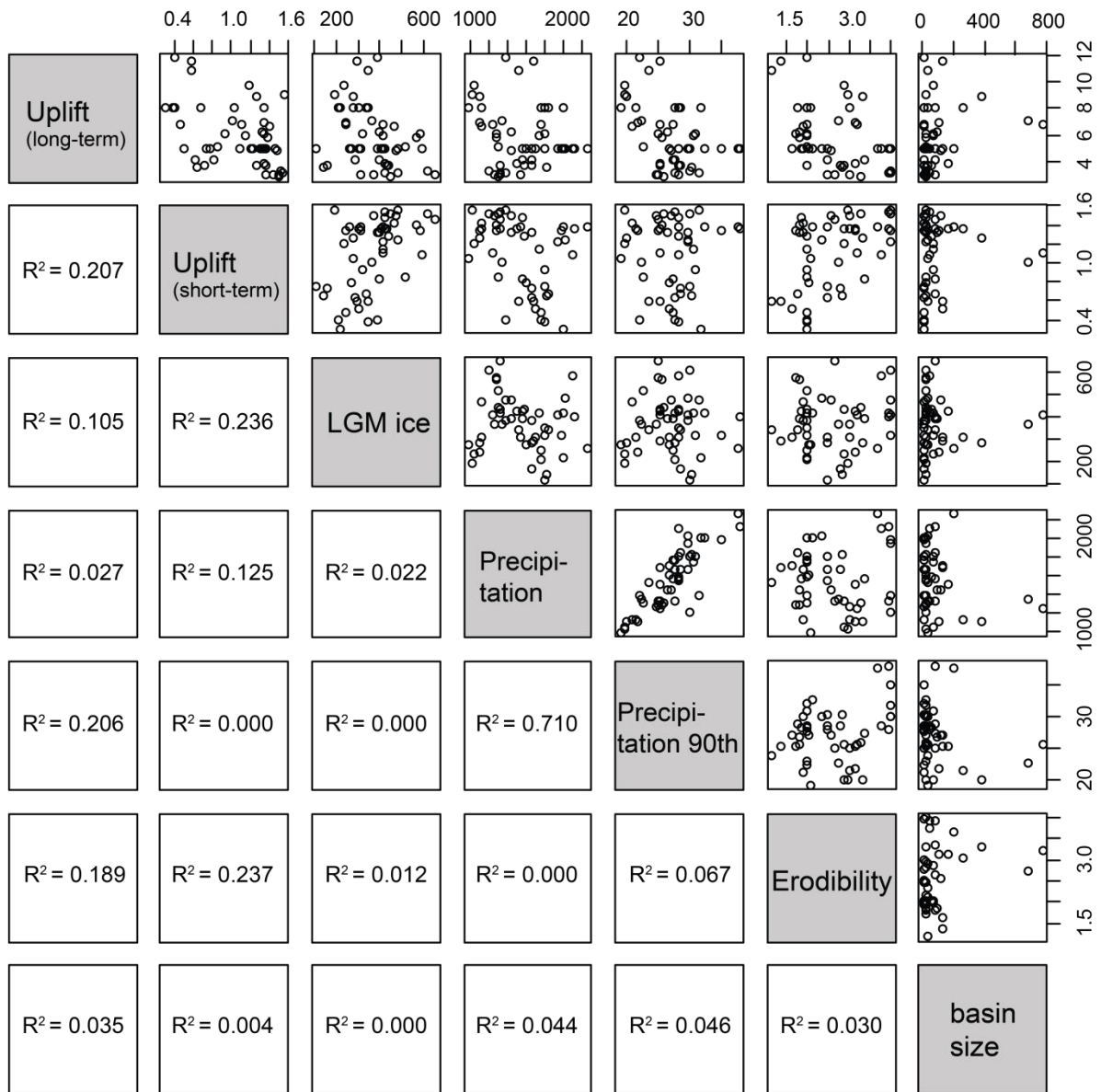
890 Figure 6



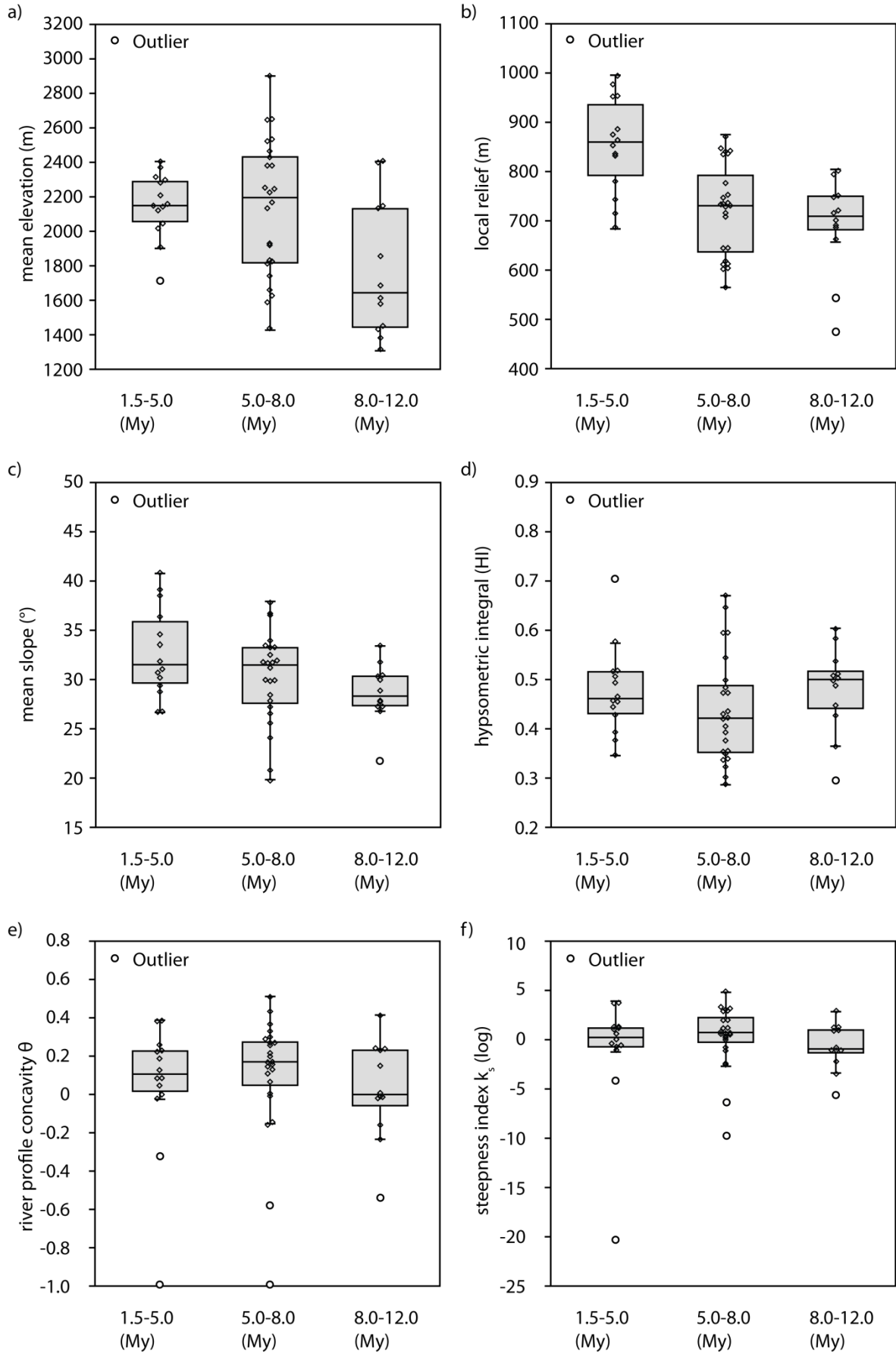
891



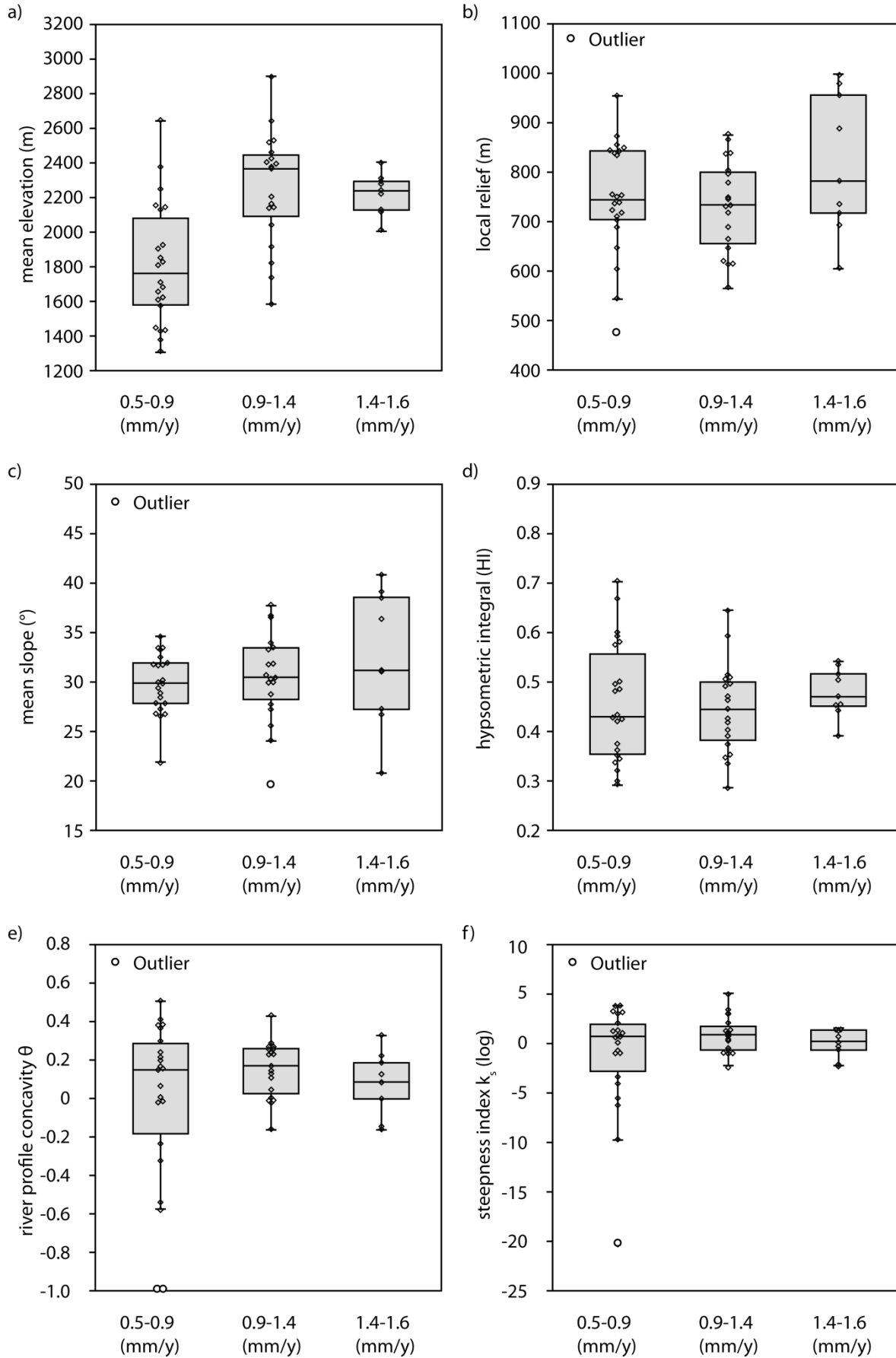
892 Figure 7



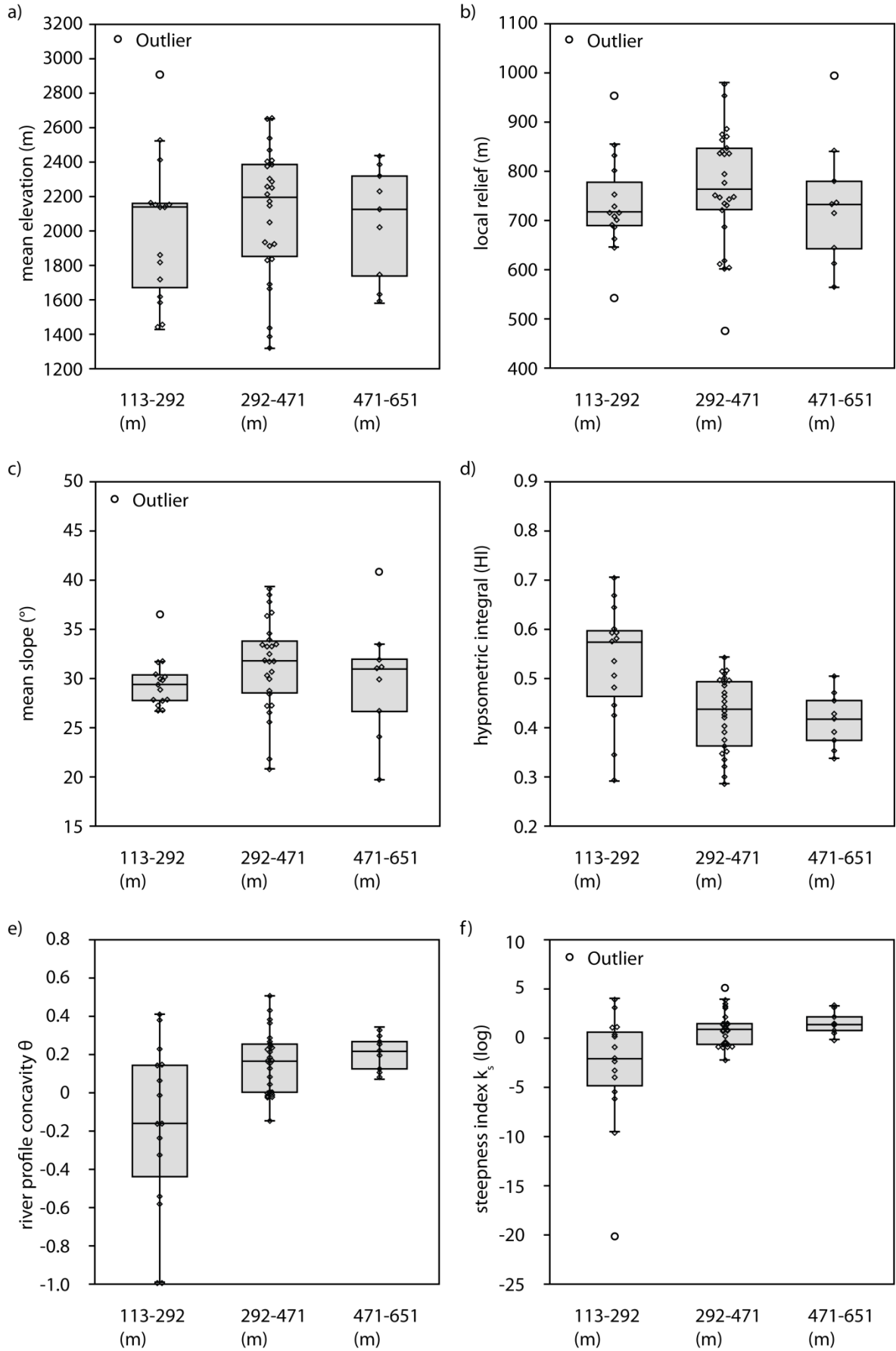
893

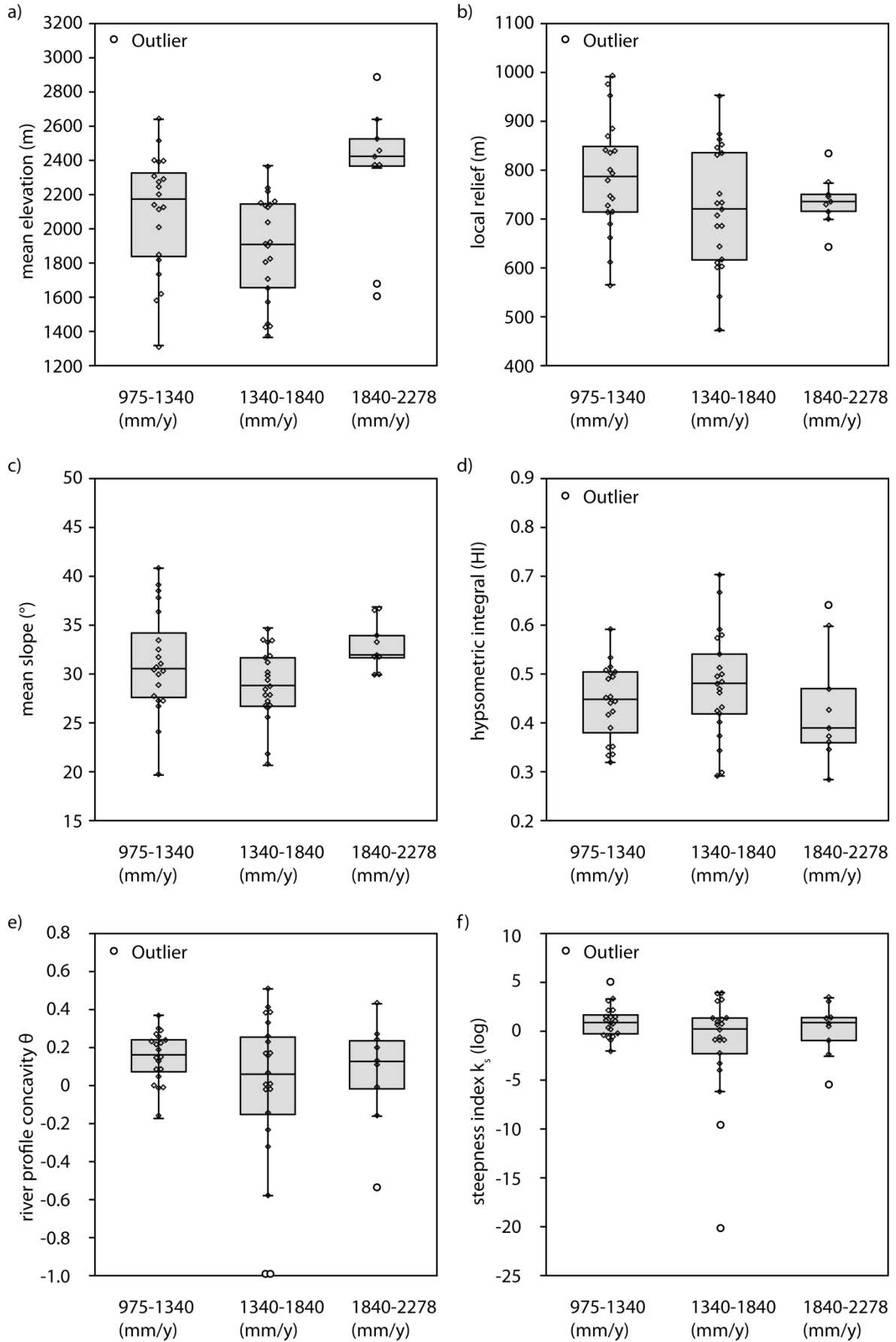


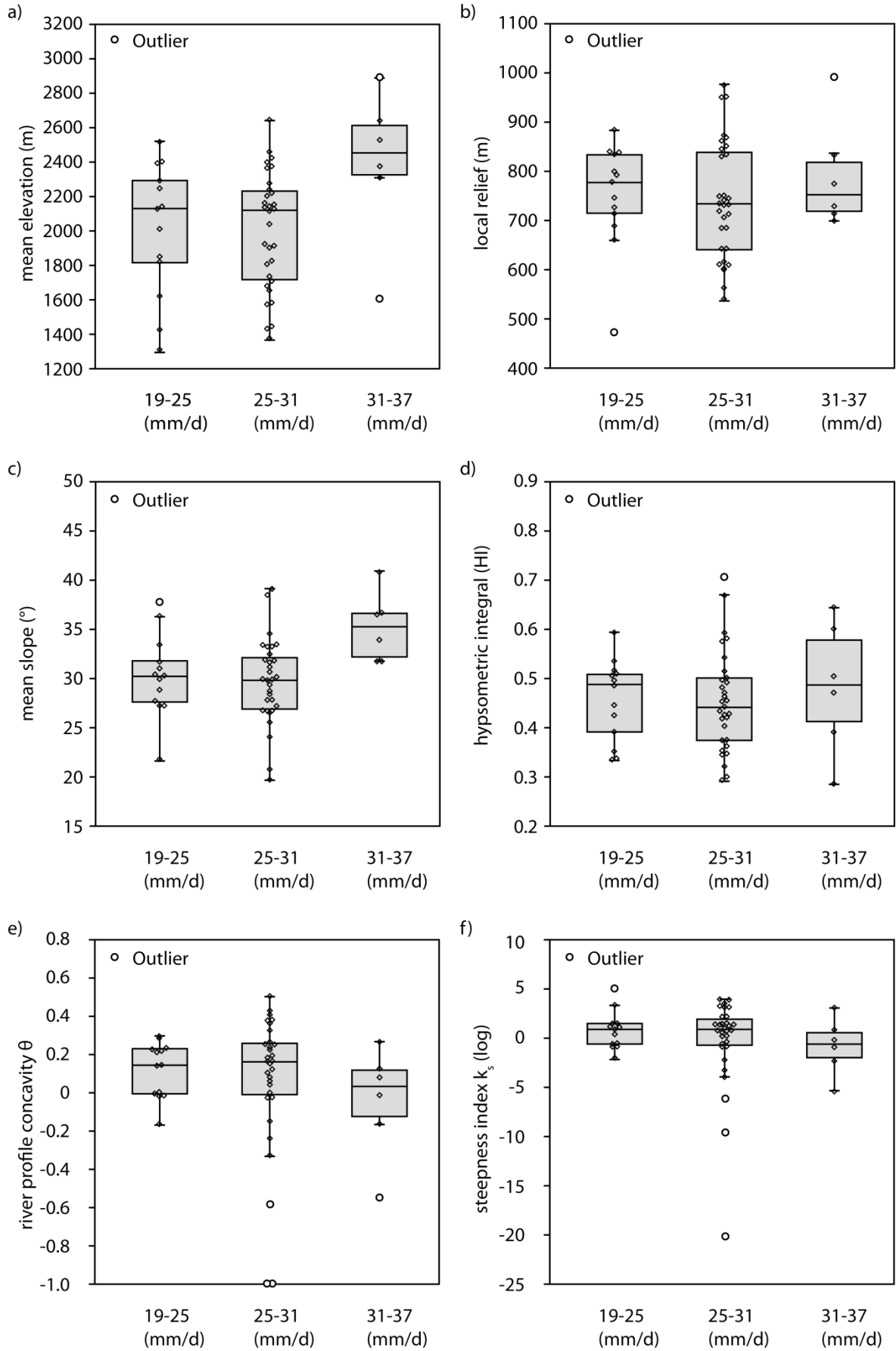
896 Figure 9

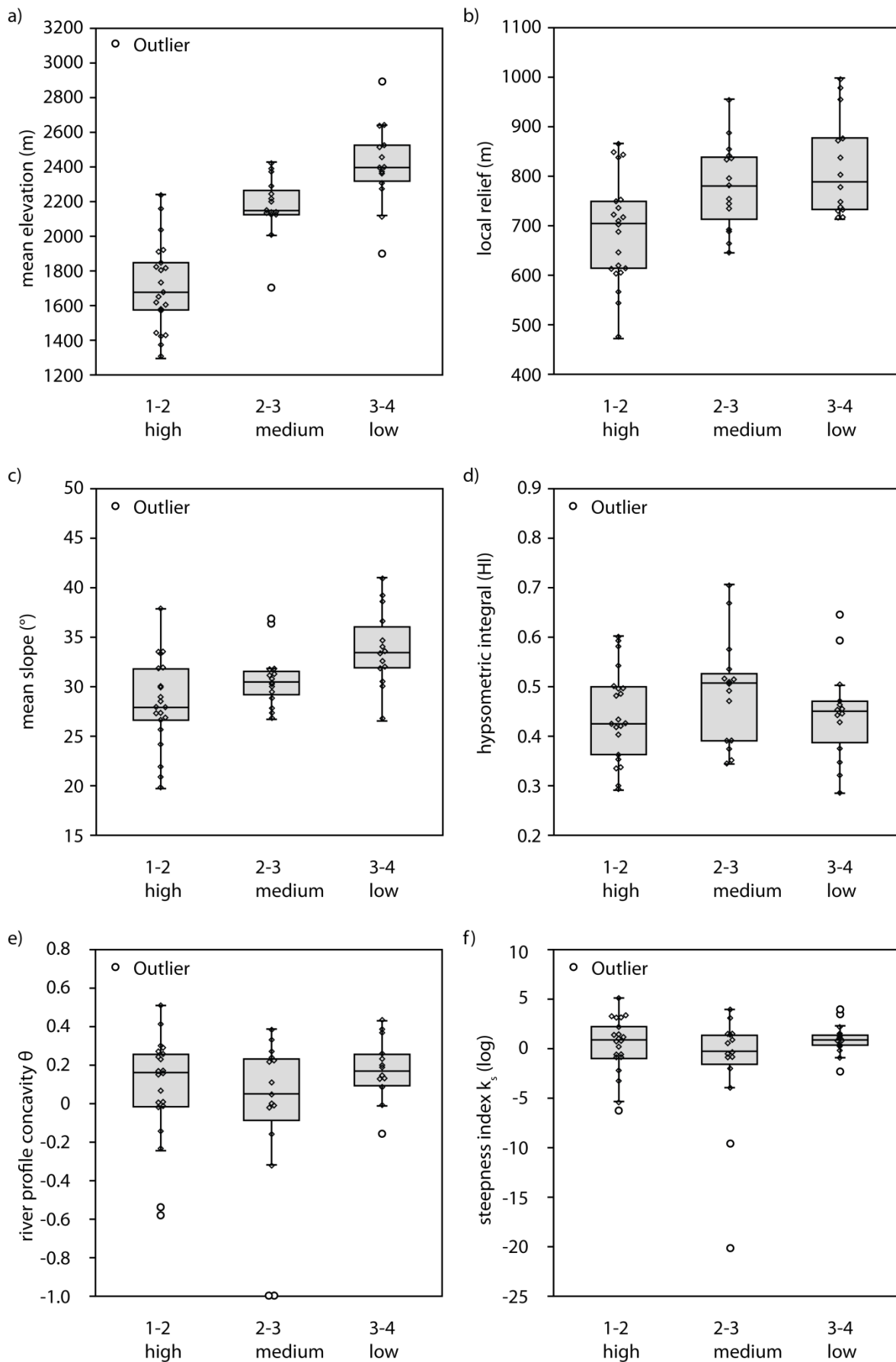


897

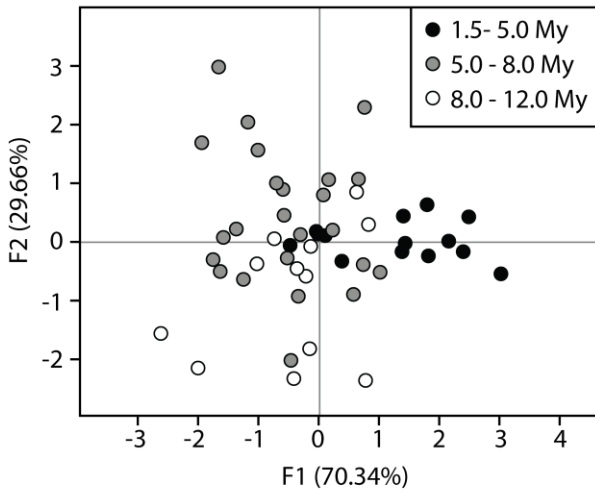




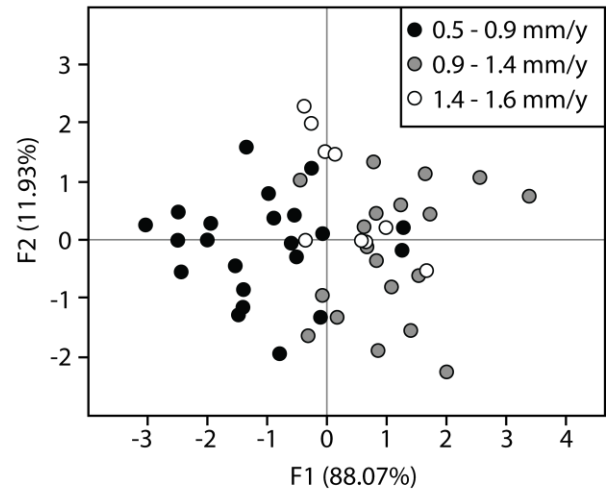




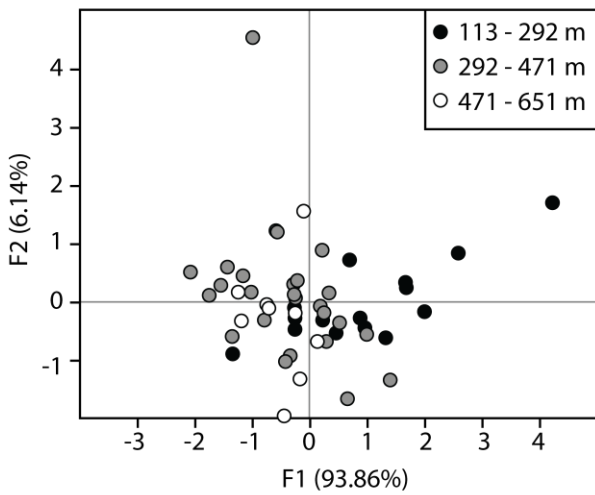
a) LDA: Apatite FT cooling ages



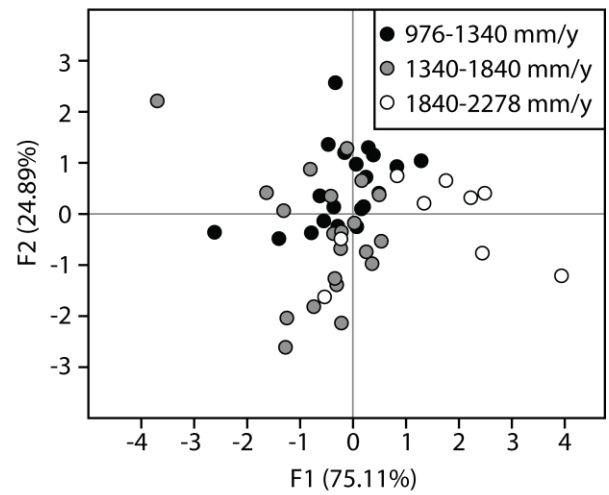
b) LDA: Recent surface uplift



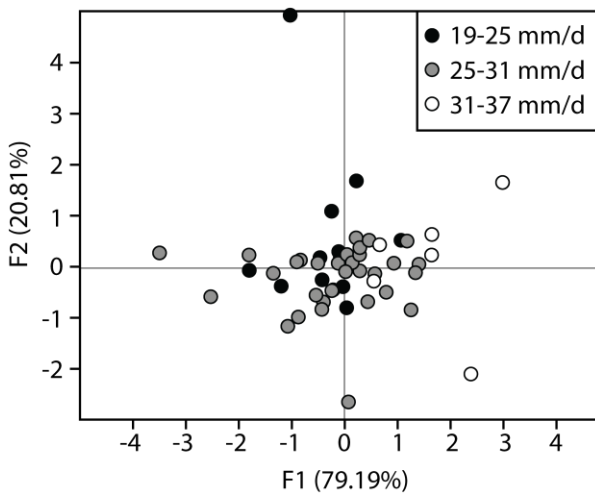
c) LDA: LGM ice thickness



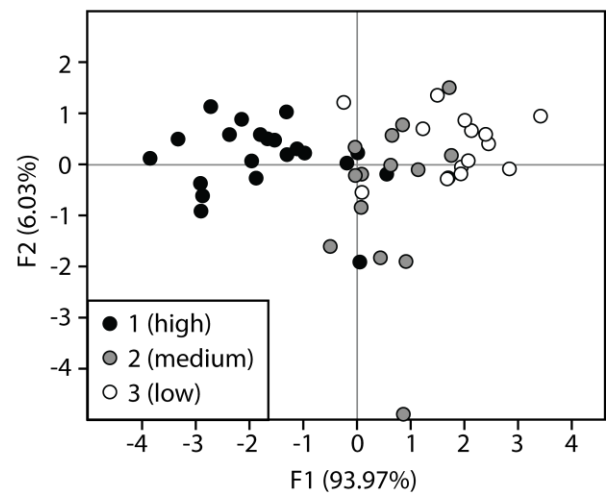
d) LDA: Precipitation amount



e) LDA: Precipitation intensity

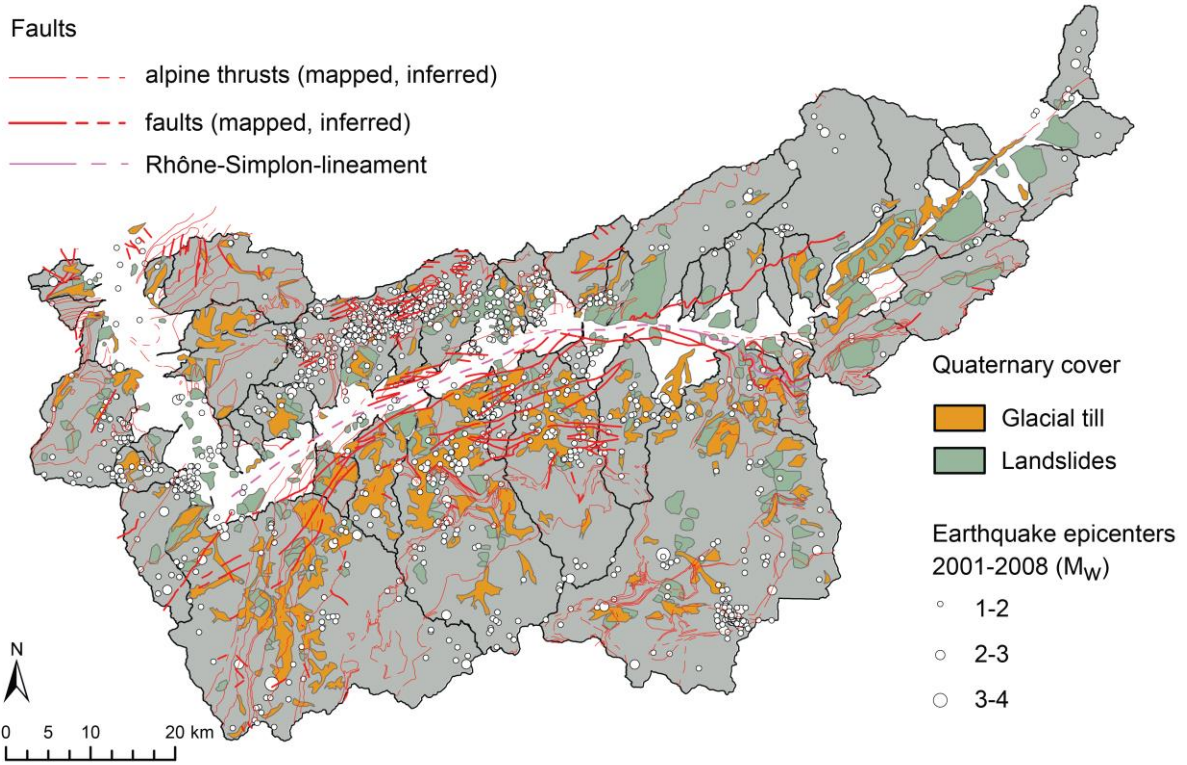


f) LDA: Erodibility





908 Figure 15



909